Global and Planetary Change 168 (2018) 78–97

Contents lists available at ScienceDirect

Global and Planetary Change

journal homepage: www.elsevier.com/locate/gloplacha

Research article

How have daily climate extremes changed in the recent past over northeastern Argentina?

Miguel A. Lovino[a,*], Omar V. Müller[a], Ernesto H. Berbery[b], Gabriela V. Müller[a]

[a] Consejo Nacional de Investigaciones Científicas y Técnicas (CONICET), Centro de Variabilidad y Cambio Climático (CEVARCAM), Facultad de Ingeniería y Ciencias Hídricas, Universidad Nacional del Litoral, Ciudad Universitaria, Ruta Nacional N° 168 - Km 472,4, 3000 Santa Fe, Argentina
[b] Earth System Science Interdisciplinary Center, Cooperative Institute for Climate and Satellites, University of Maryland, College Park, College Park, MD 20742, USA

ARTICLE INFO

Keywords:
Climate extremes
Intense precipitation
Wet/dry spells
Frost days
Heat waves
Reanalyses

ABSTRACT

Changes in climate extremes affect socioeconomics and natural systems in northeastern Argentina (NEA) and may increase its vulnerability leading to unprecedented disasters. This study investigates the long-term changes and interannual variability of daily temperature and precipitation climate extremes and assesses to what extent global reanalyses reproduce the observed variability in the recent past. Datasets include quality-controlled observations (1963–2013) and ERA-Interim and NCEP2 reanalyses (1979–2011). Climate extremes are characterized spatially and temporally by 15 indices proposed by the Expert Team on Climate Change Detection and Indices. The leading modes of the area-averaged index time series were obtained by means of a Singular Spectrum Analysis, while the spatial distribution of mean changes was estimated by fitting nonparametric linear trends to each index time series.

The results show that temperature extremes are changing towards warmer conditions. The number of warm days has been increasing since 1990 while the number of cold days has been decreasing. Warm and cold nights show a significant signal of warming that seems to be stabilizing in recent decades. Heat waves almost double the frequency and duration of cold waves, and the duration of heat waves increased while cold spells decreased in last decades. Longer heat waves are related to longer dry spells. On the other hand, the number of frost days remained stable although they exhibit high interannual and decadal variability. As well, intense precipitation events in most of the region increased steadily since 1970. The annual maximum amount of 1-day and 5-day precipitation events increased from the 1970s to the 2000s, stabilizing in recent years.

The ERA-Interim and NCEP2 reanalyses represent climate extremes with different success. ERA-Interim can recognize temperature extremes in time and space, while the older NCEP2 presents systematic positive errors and has some difficult to replicate the interannual variability of the number of summer days. Both reanalyses reproduce dry spells and the annual maximum 5-day precipitation with large biases, which are particularly noticeable at each observation station. Although reanalyses would be expected to add information for climate extremes in areas of scarce observations like northeastern Argentina, they still need to be used with great caution and only as a complement to observations, especially in studies focusing on precipitation extremes.

1. Introduction

Extreme weather and climate events affect ecosystems, disrupt food production and water supply, and negatively impact human settlements causing morbidity and mortality (Field et al., 2014). Increases in extreme events, including their frequency, intensity, spatial extent, and duration may further affect the vulnerability and exposure of ecosystems and human systems. Evidence suggests that temperature extremes have changed towards warmer conditions over most land areas of the world during the past 60 years (Seneviratne et al., 2012; Donat et al., 2013). The number of warm days and warm nights has increased, the number of cold days and cold nights has decreased, and either the length or number of heat waves has increased at the global scale (Seneviratne et al., 2012 and references therein). Although not as statistically significant as for temperature, the number of heavy precipitation events over land areas has increased (Alexander et al., 2006; Seneviratne et al., 2012) and are far more common than regions where the number has decreased (Donat et al., 2013). The changes in extreme events may impact negatively the sustainability of economic development and living conditions requiring the development of coping mechanisms to manage the associated risks (CCSP, 2008). Thus, the success in designing coping strategies depends on our understanding of the low frequency climate changes affecting extremes (Klein Tank et al., 2009).

* Corresponding author at: CONICET, CEVARCAM, FICH, UNL, Ciudad Universitaria, Ruta Nacional N° 168 – Km 472.4, CC 217, 3000 Santa Fe, Argentina.
E-mail address: mlovino@unl.edu.ar (M.A. Lovino).

https://doi.org/10.1016/j.gloplacha.2018.06.008
Received 26 May 2017; Received in revised form 15 June 2018; Accepted 19 June 2018
Available online 21 June 2018
0921-8181/ © 2018 Elsevier B.V. All rights reserved.

In South America during the last decade (2007–2016), extreme weather and climate events have led to about 7000 fatalities, more than 58 million people affected, and estimated losses of US$ 24 billion (Guha-Sapir et al., 2015). Frequent and intense precipitation extremes have favored recurrent floods in urban and rural areas (Magrin et al., 2014). According to the IPCC (2012) and Stocker et al. (2013), extreme climate events in this continent have increased in the last decades as reflected in changes in daily extremes of precipitation and temperature (e.g., Haylock et al., 2006; Rusticucci, 2012 and Skansi et al., 2013 and references therein). Towards the northern part of the South American continent not enough evidence was found to assume that changes are part of a trend (Seneviratne et al., 2012). However, towards southeastern South America a moderate confidence of a warming in temperature extremes and an increase of intense precipitation events has been detected (e.g., Fernández-Long et al., 2013; Cavalcanti et al., 2015; Carril et al., 2016 and references therein). Also consistent with global trends, the number of cold nights has decreased and warm nights has increased, the number of warm days has increased and cold days have become fewer (Rusticucci et al., 2016).

Northeastern Argentina has great economic and demographic significance as it concentrates most of the agricultural production and the population of the country. Agricultural activities are of key importance for the region's food security, helping to drive its economy, and being a main source of livelihood for the rural population (ECLAC, 2015). Hence, climate extremes affecting agriculture activities can play a significant role in the rise and fall of poverty rates. The region is particularly vulnerable to climate extremes due to its high population density and important economic activities. During the last 10 years, Argentina experienced about 16 floods or landslides with more than 100 deaths (Guha-Sapir et al., 2015). Heat waves and cold spells have increased urban mortality rates (Hardoy and Pandiella, 2009), and have affected seasonal crops by decreasing their yields (Verón et al., 2015). There is high statistical confidence that changes in climate extremes are affecting human health by increasing morbidity, mortality, and disabilities, and through the emergence of diseases in previously non-endemic regions (e.g., Winchester and Szalachman, 2009; Carbajo et al., 2012). Further research is expected to provide relevant information that can assist in the elaboration of policies related to adaptation and mitigation of the effects of climate extremes.

This study has two main objectives: first, to investigate the long-term changes and interannual variability of daily temperature and precipitation extremes, and second, under the assumption that reanalysis products should add valuable information in regions of scarce observations, to assess to what extent they reproduce the observed variability in the recent past over northeastern Argentina. The structure of the article follows: Section 2 introduces the regional context. Section 3 presents the datasets used and the methodological approach. Section 4 examines temperature-related extremes while Section 5 analyzes precipitation-related extremes. Section 6 presents a discussion and Section 7 summarizes the concluding remarks.

2. Regional context

This research focuses on northeastern Argentina (NEA), a region that covers the fertile soils of the Pampas and Chaco plains (Fig. 1a). These plains extend for 1,200,000 km^2 with a mostly flat relief and a slight slope from the northwest to the southeast (NGI, 2015). Regional topographic features favor a markedly latitudinal thermal gradient (Fig. 1d and e), with the higher temperatures towards the north (the equatorial side in the SH) and decreasing towards the south. Annual average maximum temperature ranges from 20 °C towards the south to 30 °C towards the north while annual average minimum temperature presents a less pronounced thermal gradient (10 °C to 18 °C).

Precipitation towards the northern sector of the domain north of about 20° S (Fig. 1f) is driven by the South American Monsoon System, a fundamental climate feature that controls the austral summer circulation over South America (Zhou and Lau, 1998; Nogués-Paegle et al., 2002; Marengo et al., 2012; Carvalho and Cavalcanti, 2016). The wet season is characterized by an anticyclone located approximately over the Bolivian Altiplano (Lenters and Cook, 1997), and by the Chaco thermal low, centered over northern Argentina (Nogués-Paegle et al., 2002; Marengo et al., 2012). At a more continental scale, the system extends over the ocean in what is known as the South Atlantic Convergence Zone (SACZ) (Kodama, 1992). The South American Low-Level Jet east of the Andes (SALLJ; Virji, 1981; Berbery and Collini, 2000) is a key feature of the circulation that remarkably is present throughout the year (Berbery and Barros, 2002). The SALLJ that extends from the southwestern Amazon to southeastern South America is recognized as a key factor that activates convection and precipitation in the subtropical plains of South America (Nogués-Paegle et al., 2002).

Mesoscale Convective Systems (MCSs) over Northeastern Argentina during the warm season (October–April) are frequent and account for a large percentage of the total precipitation (Laing and Fritch, 2000). During the austral cold season (May–September), the most important contribution in this region is related to activity at synoptic scale of mean latitudes (Vera et al., 2002). The conjunction of all these climate-forcing factors results in precipitation being distributed during the course of the year (Berbery and Barros, 2002). The resulting spatial pattern of the annual mean precipitation depicts a west-east gradient ranging from 900 mm/year towards the west to more than 1500 mm/year towards the northeast, as shown in Fig. 1f.

According to the literature, the variability of the southeastern South America climate at interannual to multidecadal time scales results from the superposition of several large-scale phenomena. El Niño Southern Oscillation (ENSO) is the major source of interannual variability: El Niño conditions might favor wet anomalies, intensify warms spells and reduce frost days while La Niña conditions might favor dry anomalies and increased cold events (Müller et al., 2000; Grimm and Tedeschi, 2009; Rusticucci et al., 2016). The Southern Annular Mode, and the South Atlantic and Pacific Oceans also modulate the interannual variability of extreme temperature frequencies (Barrucand et al., 2008; Loikith et al., 2017). Pacific decadal variability (PDV), the Atlantic Ocean and the SACZ are the main climate forcing factors of the southeastern South America climate variability on interannual to multidecadal time scales (Kayano and Andreoli, 2007; Mo and Berbery, 2011; Barreiro et al., 2014; Grimm et al., 2016).

3. Methodology

3.1. Datasets

In-situ observations of daily precipitation as well as daily maximum and minimum temperatures for 1963–2013 were used for the present study. They were provided by the Argentine National Weather Service and the Argentine National Institute of Agricultural Technology. About 36 stations were selected for the quality and extent of the records (see Fig. 1b and other details in Table 1). To be included, stations were required to exceed a threshold of 90% of days with data availability. As shown in Table 1, most of the selected stations (29 out of 36) had more than 95% of days with data. Missing values were filled using the normal ratio method to interpolate from nearby stations (Young, 1992). A linear regression approach was applied in exceptional cases when there was only one neighboring station with data in the period to be filled. Neighboring stations were selected according to their maximum correlation with the station to be completed. Finally, a quality control of the completed time series was carried out to identify non-systematic errors, ensure the absence of outliers and the internal consistency of the records (the latter assessed with the RHtestsV3 method developed by Wang et al., 2010).

The ERA-Interim (Dee et al., 2011) and the NCEP-DOE Reanalysis 2 (NCEP2, Kanamitsu et al., 2002) were used for the common period from 1979 to 2011. The ERA-Interim is used on a regular grid at 0.5° spatial resolution, while the NCEP2 spatial resolution is 1.875° latitude ×

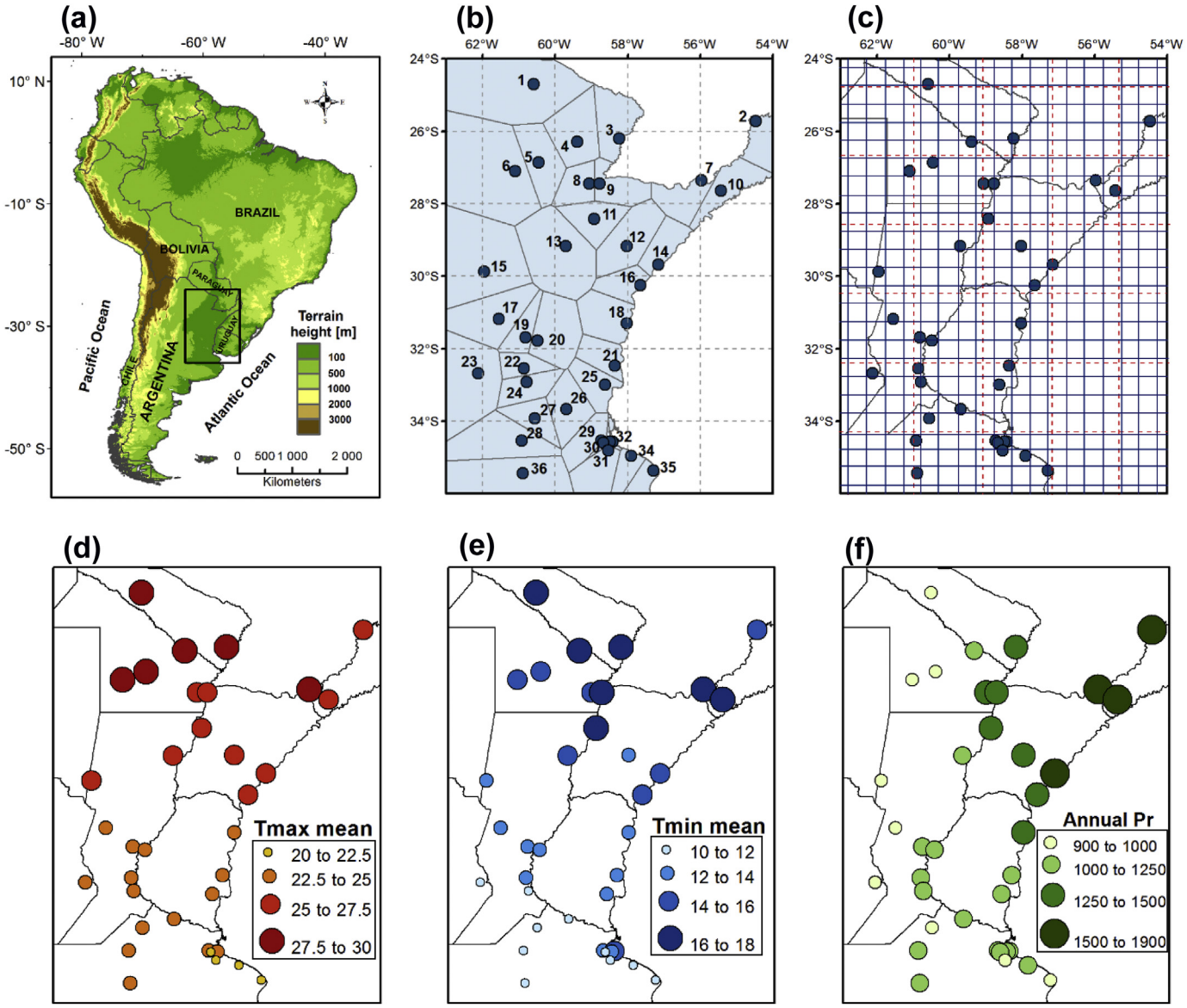

Fig. 1. (a) Topography map of South America and the main countries of southern South America. The study region in northeastern Argentina is highlighted with a black rectangle. (b) Spatial distribution of stations with long records of high-quality datasets of observed precipitation and temperature (description in Table 1) and the Thiessen polygons used to compute the areal-average of the variables. (c) Grid resolution of the reanalyses: ERA-Interim (blue full lines) and NCEP2 (red dashed lines). Climatological mean values (1963–2013 period) of the (d) annual average maximum temperature, (e) annual average minimum temperature and, (f) annual precipitation. (For interpretation of the references to colour in this figure legend, the reader is referred to the web version of this article.)

1.904° longitude (see Fig. 1c). The reanalyses offer a full coverage on areas with scarce gauge stations like the northwest portion of the domain (see Fig. 1b).

3.2. Indices of extreme climate

The more relevant NEA extreme events are those that involve precipitation and temperature. Dry and wet spells, as well as frosts, are most critical for agriculture. Heat waves are also relevant for human wellbeing. To examine these phenomena, we employ a subset of ETCCDI[1] indices that characterize the intensity, duration and frequency of climate events (Klein Tank et al., 2009 and Zhang et al., 2011). The core set of ETCCDI indices, computed from daily temperature and precipitation, was developed to detect and attribute changes and evaluate long-term variability in climate extremes. ETCCDI indices are statistically robust, can cover a wide range of climates and have a high signal-to-noise ratio. Of the 27 core indices proposed by ETCCDI, we analyze ten that are temperature-based and five based on precipitation as the most relevant for extreme events that have greatest impact in NEA (see Table 2). The indices are categorized as absolute, duration, or threshold indices (Sillmann et al., 2013): (i) absolute indices represent the intensity of extreme events, for instance, the annual maximum precipitation amounts per day; (ii) duration indices describe the length in days of wet/dry spells, or warm/cold spells; lastly, (iii) threshold indices count the number of days when a threshold is exceeded, characterizing the frequency of extreme events. Percentile-based threshold indices allow for spatial comparisons because they are independent of the spatial variability and they sample the same part of the probability distribution of a variable at each location (Zhang et al., 2011). In this study, a bootstrapping approach (Zhang et al., 2005) was applied to

[1] World Meteorological Organization (WMO) Commission for Climatology (CCl)/ CLIVAR/ JCOMM Expert Team on Climate Change Detection and Indices (ETCCDI)

Table 1
Meteorological stations used in this study with information in the 1963–2013 period.

	Station	Latitude	Longitude	Missing data (%)
1	Las Lomitas	−24.70	−60.58	0.83
2	Iguazú airport	−25.73	−54.47	5.96
3	Formosa airport	−26.20	−58.23	0.28
4	El Colorado	−26.3	−59.38	8.97
5	Roque Sáenz Peña	−26.87	−60.45	4.30
6	Las Breñas	−27.10	−61.10	2.35
7	Posadas airport	−27.36	−55.96	3.41
8	Resistencia airport	−27.45	−59.05	6.51
9	Corrientes airport	−27.45	−58.77	5.53
10	Cerro Azul	−27.65	−55.43	3.91
11	Bella Vista	−28.43	−58.92	2.03
12	Mercedes	−29.17	−58.02	6.68
13	Reconquista airport	−29.18	−59.70	1.80
14	Paso de los Libres airport	−29.68	−57.15	2.90
15	Ceres airport	−29.88	−61.95	5.83
16	Monte Caseros airport	−30.26	−57.65	0.33
17	Rafaela	−31.18	−61.55	0.84
18	Concordia airport	−31.30	−58.02	0.18
19	Sauce Viejo airport	−31.70	−60.82	0.50
20	Paraná airport	−31.78	−60.48	0.14
21	Concepción del Uruguay	−32.48	−58.35	4.16
22	Oliveros	−32.55	−60.85	0.47
23	Marcos Juárez	−32.68	−62.12	0.12
24	Rosario airport	−32.92	−60.78	0.78
25	Gualeguaychú airport	−33.00	−58.62	0.79
26	San Pedro	−33.68	−59.68	5.40
27	Pergamino	−33.93	−60.55	4.00
28	Junín airport	−34.55	−60.92	0.02
29	San Miguel	−34.55	−58.73	2.54
30	Aeroparque airport	−34.57	−58.42	1.82
31	Buenos Aires	−34.58	−58.48	0.09
32	Castelar	−34.60	−58.67	0.21
33	Ezeiza airport	−34.82	−58.53	3.11
34	La Plata airport	−34.96	−57.90	3.83
35	Punta Indio	−35.37	−57.28	4.15
36	9 de Julio airport	−35.45	−60.88	1.25

remove inhomogeneities near the beginning and end of the period in percentile-based indices, avoiding possible biases in the trend estimation.

The indices were evaluated in space and time. The most recent normal period of the time series, 1981–2010, was selected as the base period for the calculation of percentile indices and to compute anomalies of the other indices (in agreement with Zhang et al., 2011 and Skansi et al., 2013). We have verified that the choice of a different normal period (e.g. 1971–2000) and even the full data period (1963–2013) has negligible effects on the results with changes in the indices of less than 2%. To depict their spatial distribution, the mean climatology values of the observation-based and reanalysis-based indices were estimated as the average over their corresponding available periods, i.e., 1963–2013 and 1979–2011 respectively.

Area-averaged time series were computed using the Thiessen Polygons method (Okabe et al., 2000) in each time step to take into account the uneven spatial distribution of the stations (see Fig. 1b). This method calculates station weights based on the relative areas of each measurement station in the Thiessen polygon network (Fig. 1b). The individual weights are multiplied by the station observation index and the values are summed to obtain the areal average index in each time step.

3.3. Trends and variability modes of climate extreme indices

A Singular Spectrum Analysis (Ghil et al., 2001; Wilks, 2006) was employed to obtain the trends and leading modes of the area-averaged time series of each index. We focus on nonlinear trends, which allow assessing the temporal evolution of long-term changes in extreme climate events. The SSA method also detects oscillatory modes that can provide important information of the temporal variability of the climate-related extremes.

The SSA method describes the variability of a time series by its eigenvalue decomposition into temporal-empirical orthogonal functions (T-EOFs, eigenvectors) and temporal-principal components (T-PCs). Each T-PC represents a filtered version of the original time series with a portion of the variance associated with its corresponding eigenvalue. A

Table 2
ETCCDI indices used in this study, adapted from Donat et al. (2013) and Sillmann et al. (2013). TX_{ij} and TN_{ij} are the daily maximum and minimum temperature respectively on day i in period j (where period is year except for DTR that is season). $TX_{in}90$ or $TX_{in}10$ ($TN_{in}90$ or $TN_{in}10$) are the calendar day 90th or 10th percentile of daily maximum (minimum) temperature calculated for a 5-day window centered on each calendar day n from the base period 1981–2010.

	Index	Index name	Index definition	Unit
Temperature-based Indices				
Frequency	TX90p	Warm days	Percentage of annual days when $TX_{ij} > TX_{in}90$	% of days
	TX10p	Cold days	Percentage of annual days when $TX_{ij} < TX_{in}10$	% of days
	TN90p	Warm nights	Percentage of annual days when $TN_{ij} > TN_{in}90$	% of days
	TN10p	Cold nights	Percentage of annual days when $TN_{ij} < TN_{in}10$	% of days
	SU25	Summer days	Annual number of days when $TX_{ij} > 25\,^{\circ}C$	days
	TR	Tropical nights	Annual number of days when $TN_{ij} > 20\,^{\circ}C$	days
	FD	Frost days	Annual number of days when $TN_{ij} < 0\,^{\circ}C$	days
Intensity	DTR	Diurnal temperature range	Mean difference between daily maximum and daily minimum temperature: If I represents the number of days in j, then $DTR_j = \sum_{i=1}^{I} TX_{ij} - TN_{ij}/I$	°C
Duration	WSDI	Warm spell duration indicator	Annual number of days with at least 6 consecutive days when $TX_{ij} > TX_{in}90$	days
	CSDI	Cold spell duration indicator	Annual number of days with at least 6 consecutive days when $TN_{ij} < TN_{in}10$	days
Precipitation-based indices				
Intensity	RX1day	Max 1-day precipitation	Annual maximum 1-day precipitation amount	mm
	RX5day	Max 5-day precipitation	Annual maximum consecutive 5-day precipitation amount	mm
	SDII	Simple daily intensity index	Annual total precipitation divided by the number of wet days (i.e., when precipitation ≥1 mm)	mm/day
Duration	CWD	Consecutive wet days	Maximum annual number of consecutive wet days (i.e., when precipitation ≥1 mm)	days
	CDD	Consecutive dry days	Maximum annual number of consecutive dry days (i.e., when precipitation < 1 mm)	days

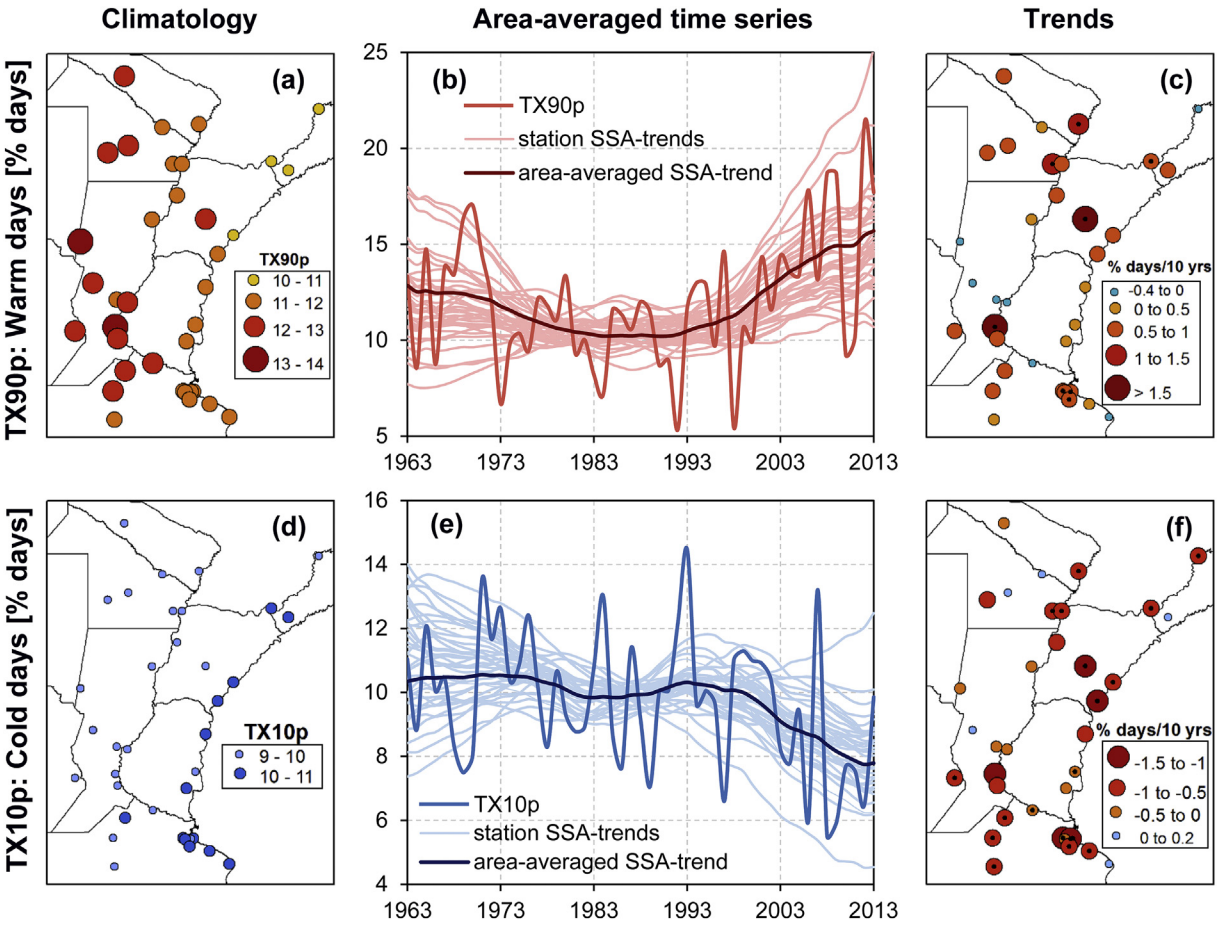

Fig. 2. Frequency of maximum temperature (daytime) climate extremes characterized by warm days (TX90p) and colds days (TX10p), defined as the percentage of annual days when Tmax > 90th percentile and Tmax < 10th percentile, respectively. Left panels (a, d): climatological mean values in the 1963–2013 period. Middle panels (b, e): the temporal evolution of the area-averaged indices and their trends. Right panels (c, f): the spatial distribution of the linear trends. Warm colors (yellow to red) indicate a shift towards warmer conditions while cold colors (light blue to blue) towards colder conditions. Stations highlighted with a black dot indicate a significant linear trend, at least at the 95% confidence level. (For interpretation of the references to colour in this figure legend, the reader is referred to the web version of this article.)

quasi-oscillatory structure can be found when two consecutive eigenvalues are nearly equal and their associated T-PCs are in quadrature. A nonlinear trend is obtained when the estimation error of a leading eigenvalue, here computed following Ghil and Vautard (1991), does not overlap with other eigenvalues and its corresponding T-PC is slowly varying and uncorrelated with other T-PCs (Vautard, 1995; Wilks, 2006). Finally, a significance test against a red noise null-hypothesis using a Monte Carlo method (Allen and Smith, 1996) with an ensemble of 1000 independent realizations was applied to distinguish significant T-PCs at the 95% confidence level.

The choice of the window length M in the SSA is crucial since it limits the longer periods that the SSA can resolve. Window length should not exceed one third of the time series length to adequately represent cycles between M/5 and M (Vautard, 1995). Considering the length of the data period available (N = 51 years), we use a window length M = 10 years. Thus, in this study, interannual variability represents the spectrum between 2 and 10 years (following Krepper and Garcia, 2004 and Krepper et al., 2006). With the window length of M = 10 years chosen here, the SSA-method cannot identify periods at decadal-to-multidecadal time scales. Our analysis will thus focus on nonlinear trends and frequencies of interannual variability cycles.

In cases when the SSA method does not clearly detect nonlinear trends, i.e. when the errors of the eigenvalues overlap preventing the separation of a significant trend signal, a 10-yr moving average, consistent with M = 10 years, was used to represent the low frequency variability. Ten-year moving averages filter signals with frequencies higher than 10 years and represent in a simpler way the low frequency behavior of the time series.

Changes in extreme climate events at each station were assessed by fitting linear trends to the indices in the 51-year period. The magnitudes of the trends were computed adapting the nonparametric Kendall's tau based slope estimator (Sen, 1968) and using the method originally proposed by Zhang et al. (2000) and later refined by Wang and Swail (2001). Trends of all indices were tested for statistical significance at the 95% confidence level following the approach of Bronaugh and Werner (2013).

3.4. Reanalyses skill evaluation

The skill of ERA-Interim and NCEP2 to reproduce temperature and precipitation extremes is assessed, first, contrasting the spatial and temporal climatology fields against observations, and second, using objective statistical metrics. The metrics used are the Pearson correlation coefficient (r), the mean bias error (MBE), and the root mean square error (RMSE). A definition of these metrics can be found in Déqué (2012).

Northeastern Argentina presents an irregular distribution of the observation stations, as noted above (see Fig. 1b). Therefore, comparisons between grid cell products with station observations necessarily involve interpolations, which introduces new errors (Wang and Zeng,

2012). To minimize these interpolation errors, we follow the approach in Wang and Zeng (2012), Jones et al. (2016), Yang and Kim (2017) and Zhang et al. (2017) by comparing data from each station with those from a reanalysis grid cell covering this station. It should be noted that given the lack of topographic characteristics of the region (see Fig. 1a), there are no sharp gradients and the variations of the climatic variables are largely unaffected by their spatial resolution.

The ability of the reanalyses to represent temperature extremes is evaluated by means of three fixed-threshold indices: summer days, tropical nights and frost days (SU25, TR and FD respectively; see their definitions in Table 2). These indices were selected for two reasons: first, they avoid the complexity of percentile-based indices, which are difficult to replicate in reanalysis (estimated but not shown; see also Sillmann et al., 2013), and second, because they are relevant to the agro-industrial activities in the region. For precipitation extremes, the annual maximum 5-day amounts (RX5day) and the annual maximum consecutive dry days (CDD) are evaluated (see the indices definitions in Table 2). As suggested by Sillmann et al. (2013), reanalyses tend to underestimate the magnitude of extreme precipitation events characterized by the annual maximum 1-day amount (RX1day, Table 2), but they may have greater ability to reproduce the CDD and RX5day because dry conditions and 5-day precipitation events are usually of larger spatial scale than daily extreme precipitation events.

4. Temperature-related climate extremes

4.1. Maximum-temperature frequency extremes

The frequency of days per year when the maximum temperature exceeds the 90th percentile (TX90p) will be referred to as warm days. The frequency of days when the maximum temperature is below the 10th percentile (TX10p) will be referred to as cold days. The climatology of warm days (Fig. 2a) has an almost longitudinal gradient that ranges from 14% of days per year towards the west to 10% towards the northeast. The warm days are influenced by interannual variability with a periodicity close to 9 years (Table 3) which explains 30% of the variance of the total time series. Fig. 2b (and Table 3) also reveals a nonlinear trend of the frequency of warm days, which had slightly decreased before the 1990s, but since then it has experienced a steady increase of about 5%. Despite the dispersion among the trends of TX90p for all stations (thin lines in Fig. 2b), they exhibit a common behavior. The spatial distribution of the trends in Fig. 2c reveals that most stations have increases of warm days, particularly towards the northeast. Only a few stations (7 out of 36) experienced a decrease, and it was non-significant.

Days with the maximum temperature in the lowest 10th percentile (cold days), shown in Fig. 2d, are less frequent than warm days and almost uniform for the region, with a slight increase towards the east from 9% to 11% of cold days in a year. The area-averaged frequency of colds days presented in Fig. 2e reveals a decrease from 10% to 7.5% of days per year since about 1990 with an important interannual variability. The spatial distribution of the linear trends presented in Fig. 2f shows the largest decrease of cold days towards the east, where cold days are more frequent.

4.2. Minimum-temperature frequency extremes

Fig. 3 presents the indices characterizing the frequency of minimum-temperature extremes. The indices TN90p and TN10p (Table 2) describe respectively the percentage of nights when minimum temperature was in the 90th percentile (warm nights) and the percentage of nights when it was in the lowest 10th percentile (cold nights). The annual mean climatology of warm nights (Fig. 3a) presents values between 9% and 12% of days without a clear spatial pattern. Fig. 3b indicates that warm nights exhibit an area-averaged positive nonlinear trend, more evident from the late 1960s to the early 1980s. From 1980 to 2013, the trend is also positive but with lower magnitude, being strongly influenced by interannual variability. It is of interest to examine the individual stations trends (thin lines). They exhibit smaller dispersion around the 1980s, with a marked dispersion increase during latter years. Aside from the trends, a 4-yr mode of variability explains almost 30% of the TN10p and TN90p variances (see Table 3). Fig. 3c shows that the number of warm nights presents the greatest increases towards the north (1% to 2% of days per decade), with 11 out of 19 stations with significant rising trends. Only a few stations (about 6) had a non-significant negative trend.

The frequency of cold nights (Fig. 3d) ranges from 9% to 13% of annual days, again without a well-defined spatial pattern. Their mean trend, presented in Fig. 3e, shows that there was about a 5% decrease in the frequency of cold nights from the 1960s to 1980s, that is, at the same time when an increase of about 3% was observed in the frequency of warm nights (Fig. 3b). According to Fig. 3f, the decrease in cold nights occurred in the whole region, with 21 stations having significant trends at least at the 95% confidence level.

4.3. Frost events and diurnal temperature range

Many crops are sensitive to the number of frost days (FD) and to the diurnal temperature range (DTR) defined in Table 2. These indicators of temperature-related extremes provide useful information for agricultural planning. Fig. 4 displays the climatology, areal-averaged temporal evolution and spatial distribution of local trends of these indicators. Consistent with the minimum temperature climatology (Fig. 1e), the frequency of frost days varies latitudinally, decreasing from almost 25 days per year towards the south to less than 5 days per year to the north (Fig. 4a). Frost days do not have a noticeable trend

Table 3
Summary of the main variability modes of temperature-related extremes found with SSA.

SSA results of temperature-based indices					
	Index	Index name	Components	Trend or dominant period (year/cycle)	Explained variance (%)
Frequency	TX90p	Warm days	T-PC1	Trend	27
			T-PC2 and T-PC3	8.8	30.5
	TX10p	Cold days	T-PC1	Trend	18
	TN90p	Warm nights	T-PC1	Trend	18
			T-PC2 and T-PC3	4	27
	TN10p	Cold nights	T-PC1	Trend	36
			T-PC2 and T-PC3	4	28
	FD	Frost days	T-PC1 and T-PC2	4	42.5
Intensity	DTR summer	Summer diurnal temperature range	T-PC1	Trend	21
	DTR winter	Winter diurnal temperature range	No significant modes		
Duration	WSDI	Warm spell duration indicator	T-PC1	Trend	20
	CSDI	Cold spell duration indicator	T-PC1	Trend	43.5

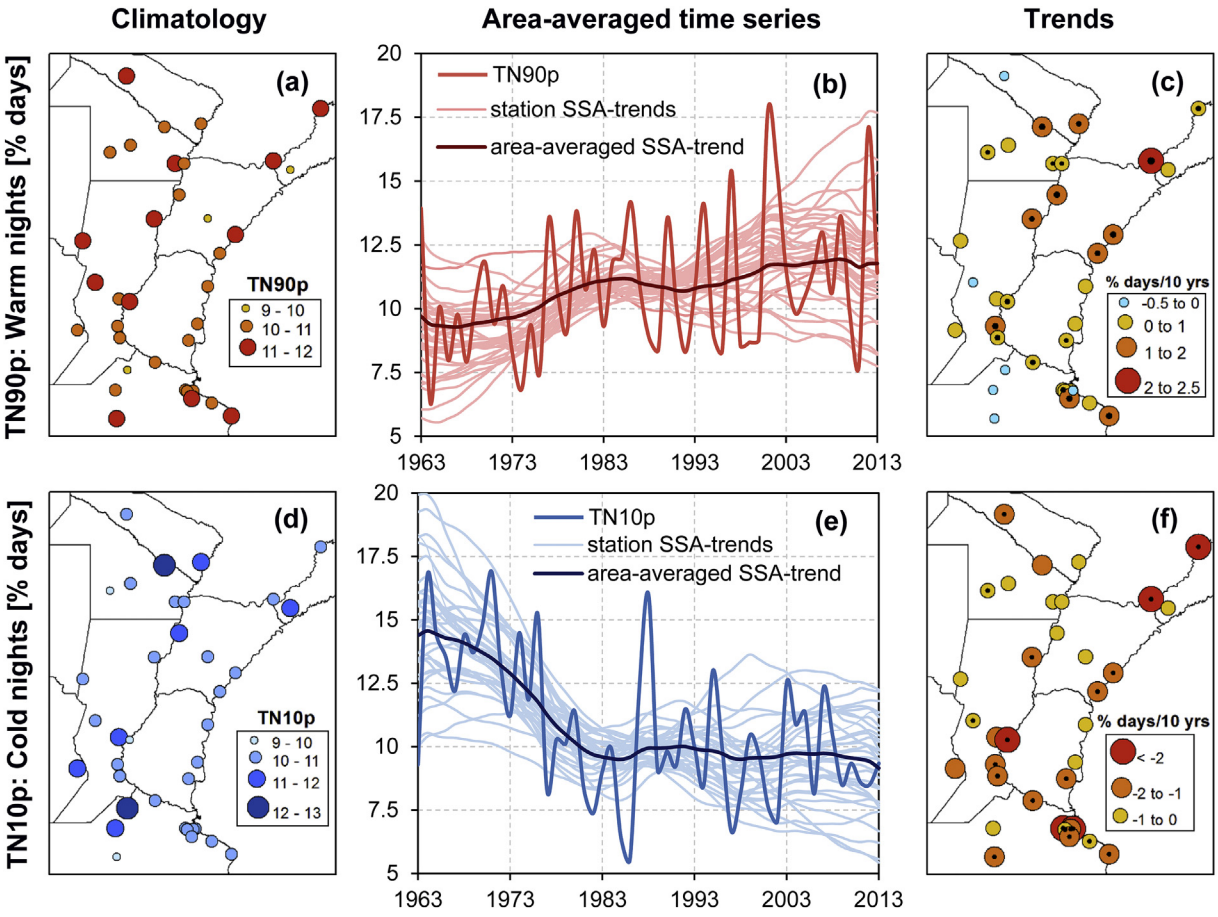

Fig. 3. Frequency of minimum temperature (nighttime) climate extremes characterized by warm nights (TN90p) and colds nights (TX10p), defined as the percentage of annual days when Tmin > 90th percentile and Tmin < 10th percentile, respectively. Left panels (a, d): climatological mean values in the 1963–2013 period. Middle panels (b, e): the temporal evolution of the area-averaged indices and their trends. Right panels (c, f): the spatial distribution of linear trends. Warm colors (yellow to red) indicate a shift towards warmer conditions while cold colors (light blue to blue) towards colder conditions. Stations highlighted with a black dot indicate a significant linear trend, at least at the 95% confidence level. (For interpretation of the references to colour in this figure legend, the reader is referred to the web version of this article.)

(Fig. 4b and c), but they do exhibit interannual and decadal variability. On interannual scales, a 4-yr mode is consistent with the cycle discussed for minimum-temperature extremes, particularly in cold nights, explaining 42.5% of the FD variance (Table 3).

During austral summer, the diurnal temperature range (DTRs) varies between 10 °C and 14 °C with highest values towards the west (Fig. 4d). The nonlinear area-averaged SSA-trend in Fig. 4e indicates that DTRs decreased substantially between the 1960s and 1970s, and remained constant from the 1980s to the present. The local trends shown in Fig. 4f exhibit negative values over most of the region, with largest negative trends of up to 0.5 °C in magnitude per decade towards the south. Almost negligible positive trends (< 0.1 °C) are found in very few stations, without any clear pattern.

During winter, the diurnal temperature range (DTRw) in Fig. 4g has a similar pattern as in summer, ranging from 14 °C towards the west to 9 °C towards the east. Changes in time of the area-averaged DTRw (Fig. 4h) reveal a decrease in the earlier period and a continued increase from the 1990s to the present. Fig. 4i suggests that the entire region experienced an increase in the DTR, with 28 out of 36 stations having positive trends.

4.4. Duration of warm and cold spells

Agriculture and human settlements may be severely affected by heat and cold waves. The warm spell duration indicator (WSDI) is defined as the annual count of days with at least six continuous days when maximum temperature exceeds the 90th percentile (see Table 2). The index for cold waves follows an equivalent definition, as it corresponds to the annual count of days with at least six continuous days that have a minimum temperature within the 10th percentile. Note that in principle WSDI and CSDI are not necessarily related to latitudinal changes, since they account for the number of days exceeding a percentile-threshold. Yet, some spatial structures can be identified. Fig. 5a-c present the mean annual frequency, duration and area-averaged temporal evolution of warm spells. It can be seen that heat waves are more frequent (Fig. 5a) but of shorter duration (Fig. 5b) towards the north, where there is up to 70% of chance of a heat wave per year with a duration of about 8 to 12 days. Towards the south, heat waves are less frequent but can last longer, up to about 16 days. The evolution of WSDI shown in Fig. 5c indicates that warm spell duration slightly decreased during the first half of the period, and then increased from the 1990s to present. The highest anomaly value of the WSDI was registered in 2008 with an average of more than 20 consecutive days, when the whole region experienced a severe drought and heat wave (Müller et al., 2014; Rusticucci et al., 2015). Indeed, some stations in the south-center registered WSDI of more than 60 days.

The cold waves (CSDI) are more frequent (Fig. 5d) and of longer duration (Fig. 5e) towards the north, where minimum temperatures are higher than in the south (see Fig. 1e). For example, the probability of having one 10-day cold wave per year is 40% while towards the colder south, the probability of a cold wave is below 20%. The temporal evolution of the area-averaged CSDI (Fig. 5f) indicates that cold spell

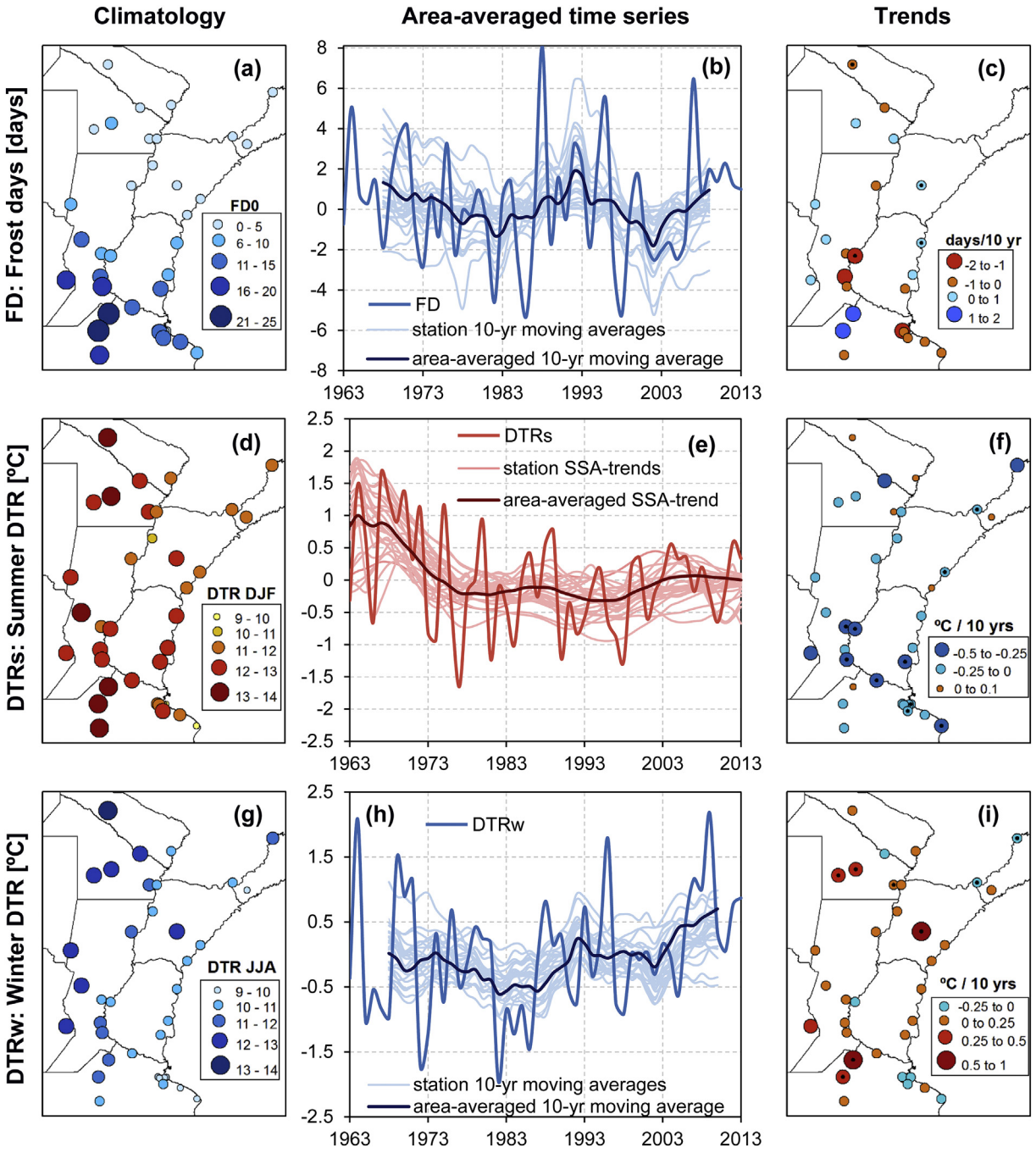

Fig. 4. Number of frost days (FD, first row) and the diurnal temperature range during summer (DTRs, second row) and winter (DTRw, third row). Left panels (a, d, g): climatological mean values in the 1963–2013 period. Middle panels (b, e, h): the temporal evolution of the area-averaged indices and their trends. Right panels (c, f, i): the spatial distribution of linear trends. Warm colors (yellow to red) indicate a shift towards warmer conditions wile cold colors (light blue to blue) towards colder conditions. Stations highlighted with a black dot indicate a significant linear trend, at least at the 95% confidence level. (For interpretation of the references to colour in this figure legend, the reader is referred to the web version of this article.)

duration decreased markedly in the mid-1960s and remained at about the same level since then. A strong decadal variability is noticed throughout the period.

4.5. Temperature-related extremes in reanalyses

So far we have examined extremes as identified by station observations which do not have a complete coverage of the study region. Global reanalysis offer full data coverage in time and space based on a global model that assimilates diverse kinds of observations. Then, it is of interest to assess whether reanalysis products can be used as a complement to observations in northeastern Argentina where there is a limited coverage of gauge stations. In this sub-section, we examine the skill of two reanalysis (NCEP2 and ERA-Interim) to reproduce maximum-temperature extremes (characterized by summer days) and minimum-temperature extremes (represented by tropical nights and frost days). In addition to the already defined FD index, the summer days index (SU25) is obtained as the annual number of days when Tmax > 25 °C; and the tropical nights index (TR) is computed as the annual number of days when Tmin > 20 °C (see details on Table 2). These two indices have a latitudinal dependence with larger values towards lower latitudes.

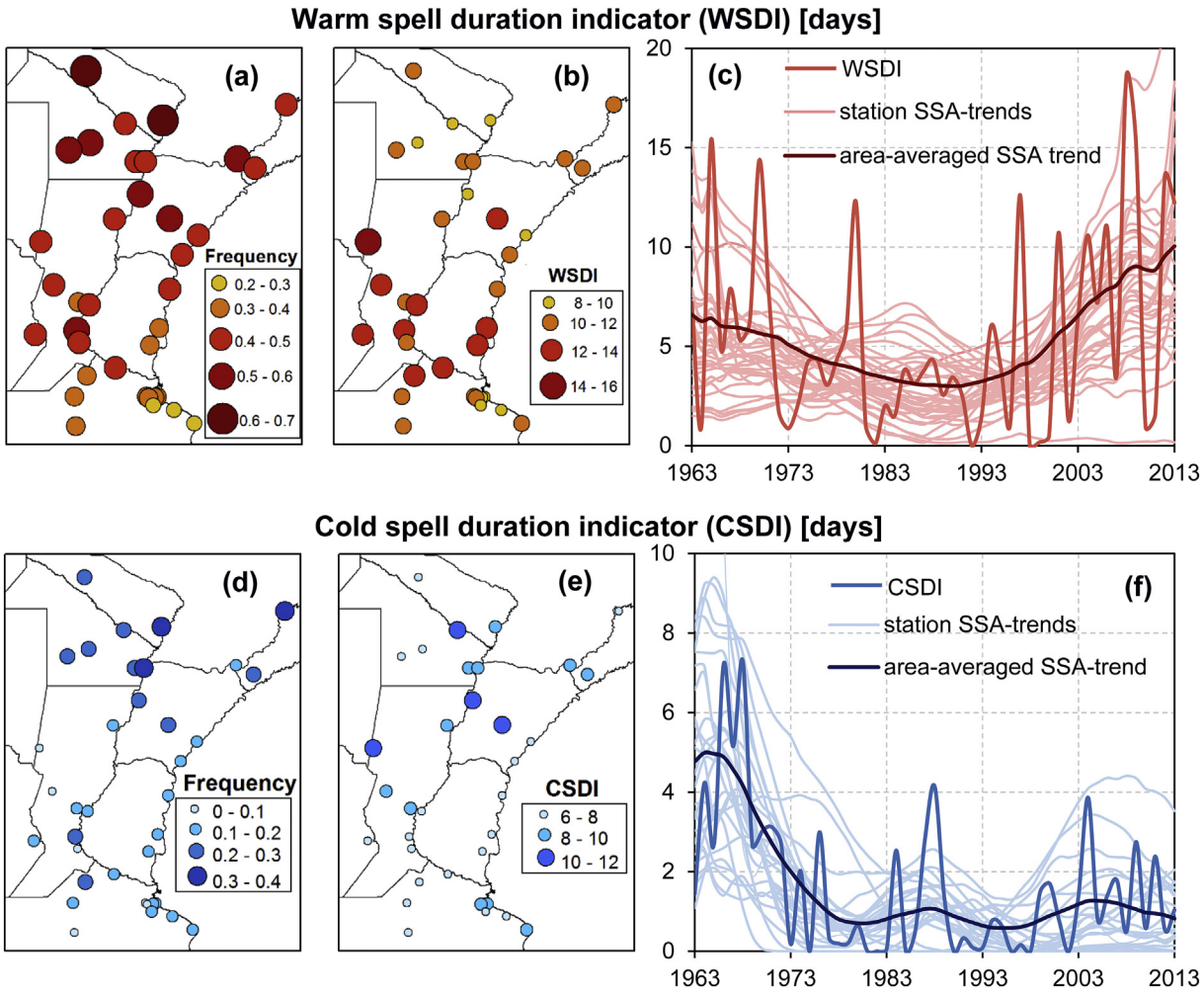

Fig. 5. Metrics of warm and cold spell duration (definitions are given in Table 2). Frequency of at least one event per year in (a) and (d); average duration in years with occurrence in (b) and (e); area-averaged time series in (c) and (f).

4.5.1. Number of summer days (SU25)

The overall characteristics of the SU25 index are presented in Fig. 6a. The spatial field from the reanalysis are superimposed by circles of the corresponding values obtained from observations. A visual inspection suggests that there is similarity between the spatial pattern identified in observations and reanalyses. NCEP2, an older reanalysis product, overestimates the field of observed summer days towards the south. According to Fig. 6a (right panel), the area-averaged SU25 estimated from ERA-Interim follows the temporal evolution of the observations-based SU25 with a mean bias error of only 3 days and a correlation coefficient close to 0.9. However, the interannual variability of the area-averaged SU25 is not properly represented by NCEP2, with a correlation coefficient of 0.51.

Statistical metrics for SU25 index computed from reanalyses at each station location are presented in Fig. 7. ERA-Interim achieves the best performance, particularly towards the south, with most correlations to observations exceeding 0.7 (see histogram below map in Fig. 7a). In contrast, the older NCEP2 shows lower values with the most frequent correlations in the range between 0.4 and 0.6 (see histogram below map in Fig. 7b).

Fig. 7c and d show that the two reanalyses have mostly positive mean bias errors, with ERA-Interim having an overestimation of up to 10 summer days in most stations. The older NCEP2 shows positive biases in the range of 10–20 days and larger. Consistently, Fig. 7e and f indicate that the most frequent RMSE values for ERA-Interim are < 20 days, while those for NCEP2 exceed 20 days.

4.5.2. Number of tropical nights (TR)

The mean fields of the number of tropical nights (days with Tmin > 20 °C) in Fig. 6b show the expected increase towards the lower latitudes in both observations and reanalysis. The two reanalyses reproduce the south-north gradient but with a larger number of tropical nights towards the south. This overestimation is more noticeable in the area-averaged time series (right panel). The observed mean value of tropical nights is 56 days, while the ERA-Interim and NCEP2 have a larger number, 102 and 112 days respectively. The time series shows that both reanalyses retain information about the interannual variability, giving correlation coefficients of 0.69 for ERA-Interim and 0.61 for NCEP2.

Fig. 8 shows that the two reanalyses represent tropical nights with less success, lower correlations, than summer days (Section 4.5.1). The histogram in Fig. 8a shows that the most frequent correlation values range between 0.4 and 0.7 for ERA-Interim while NCEP2 presents correlation values < 0.6 in the whole region (Fig. 8b). Fig. 8c and d show that the two reanalyses overestimate tropical nights although ERA-Interim has smaller biases than NCEP2 towards the south (MBE of 20–40 days for ERA-Interim and MBE of 40–60 days for NCEP2). The histograms in Fig. 8e and f indicate that ERA-Interim presents common RMSE between 20 and 40 days while the most frequent RMSEs for NCEP2 are well above the 40 days.

4.5.3. Number of frost days (FD)

As with the two previous indices, the number of frost days is largest

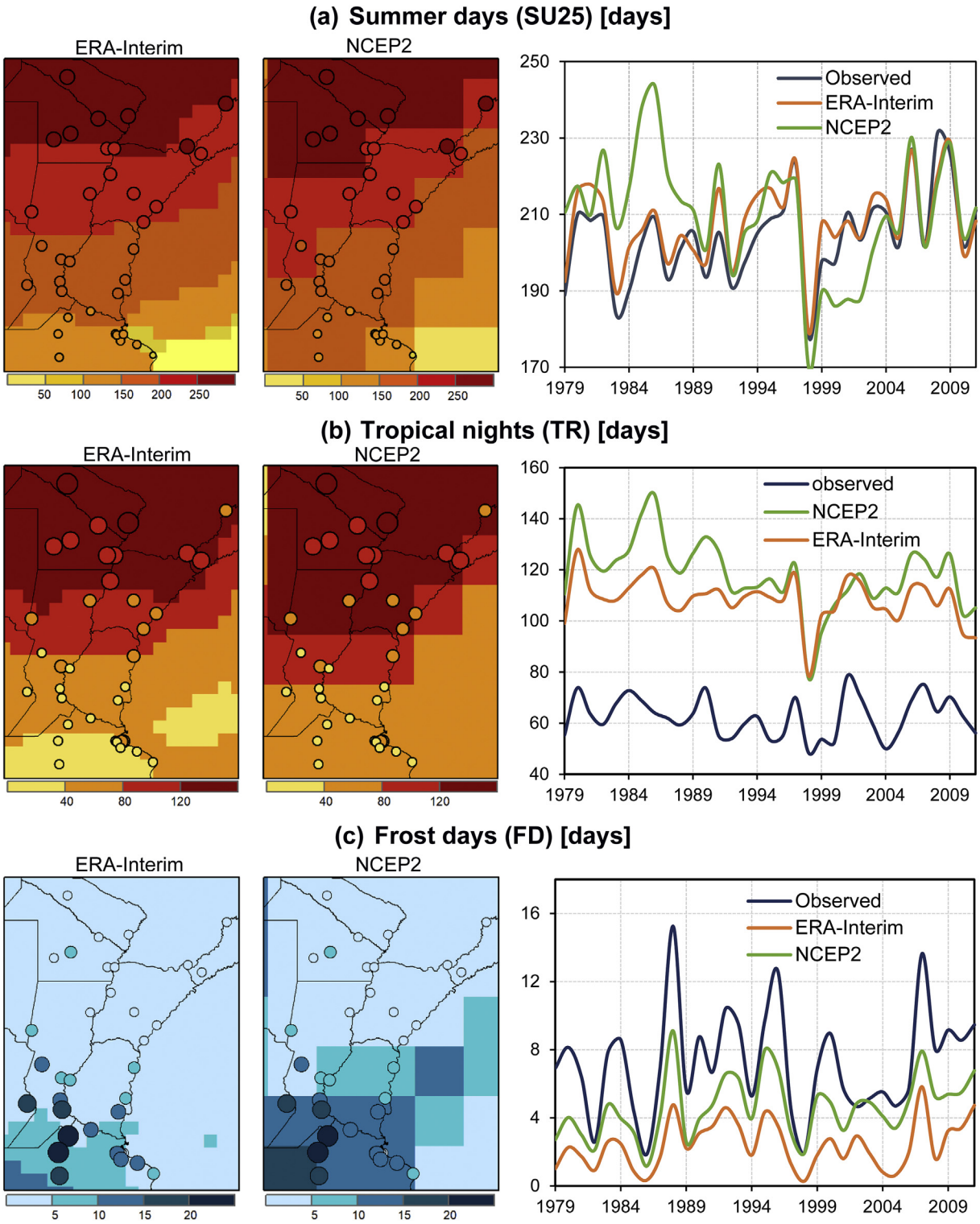

Fig. 6. (a) Summer days (SU25), (b) tropical nights (TR) and (c) frost days (FD) represented by the ERA-Interim and NCEP2 reanalyses for the period 1979–2011 and compared with observations. Spatial distribution of mean climatology values are given in the first two panels while area-averaged time series of the Argentinian territory in the third panel of each row.

towards the colder south. Fig. 6c shows that both ERA-Interim and NCEP2 tend to reproduce the spatial mean fields, but underestimate the spatiotemporal variability of frost days, particularly towards the south. Note that in the northern portion of the region, closest to the tropics, there are less than 5 frost days per year (see Fig. 6c), still, when they occur, they may severely damage crops that are of more subtropical nature. The time series of area-averaged frost days on the right panel exhibit similar variability ($r = 0.86$ for ERA-Interim and $r = 0.87$ for NCEP2) but with a systematic mean bias error of −3 days for NCEP2 and − 5 days for ERA-Interim.

Fig. 9 shows that the two reanalyses characterize frost days with similar statistical metrics: the most frequent correlation coefficients range between 0.5 and 0.7 (Fig. 9a and b) and MBE reaches values lesser than −5 days towards the south of the study region (Fig. 9c and

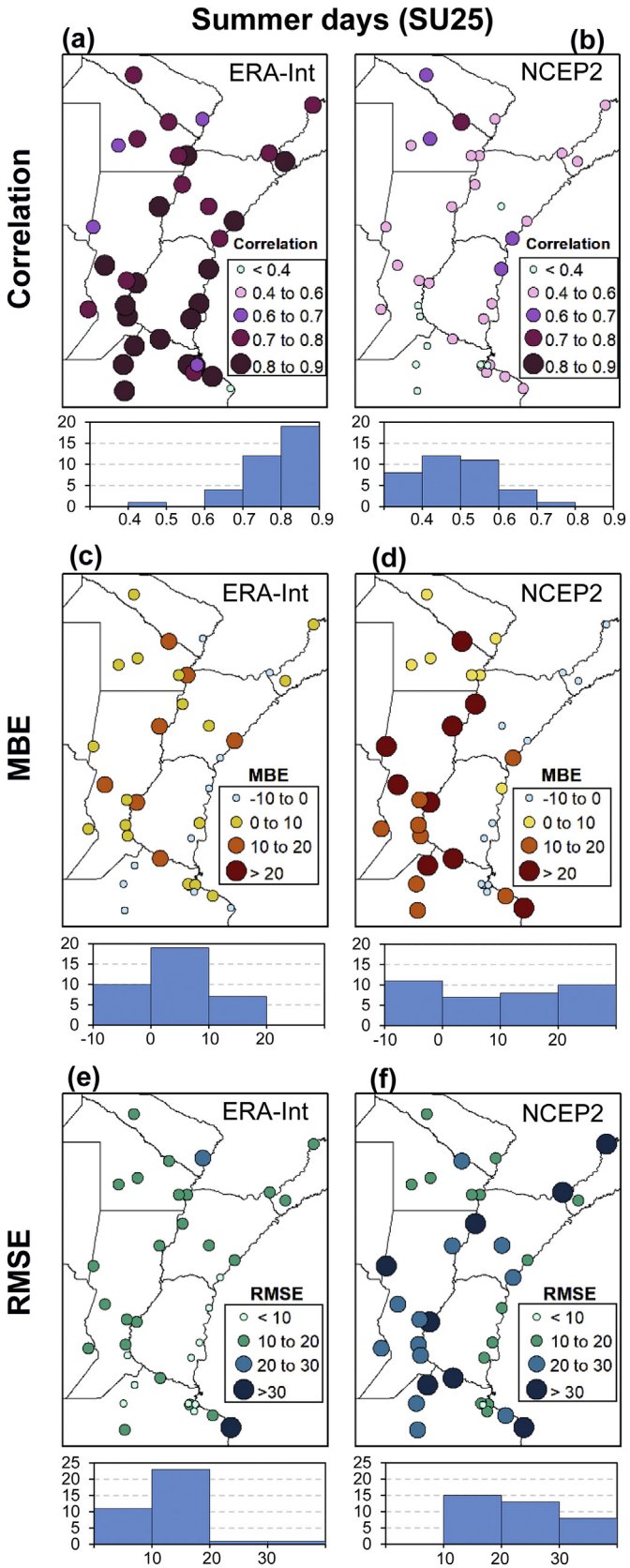

Fig. 7. Spatial distribution of the correlation coefficients (a, b), the MBE (c, d) and the RMSE (e, f) for summer days (SU25) represented by the ERA-Interim and NCEP2 reanalyses for the period 1979–2011. Histograms are provided below of each map.

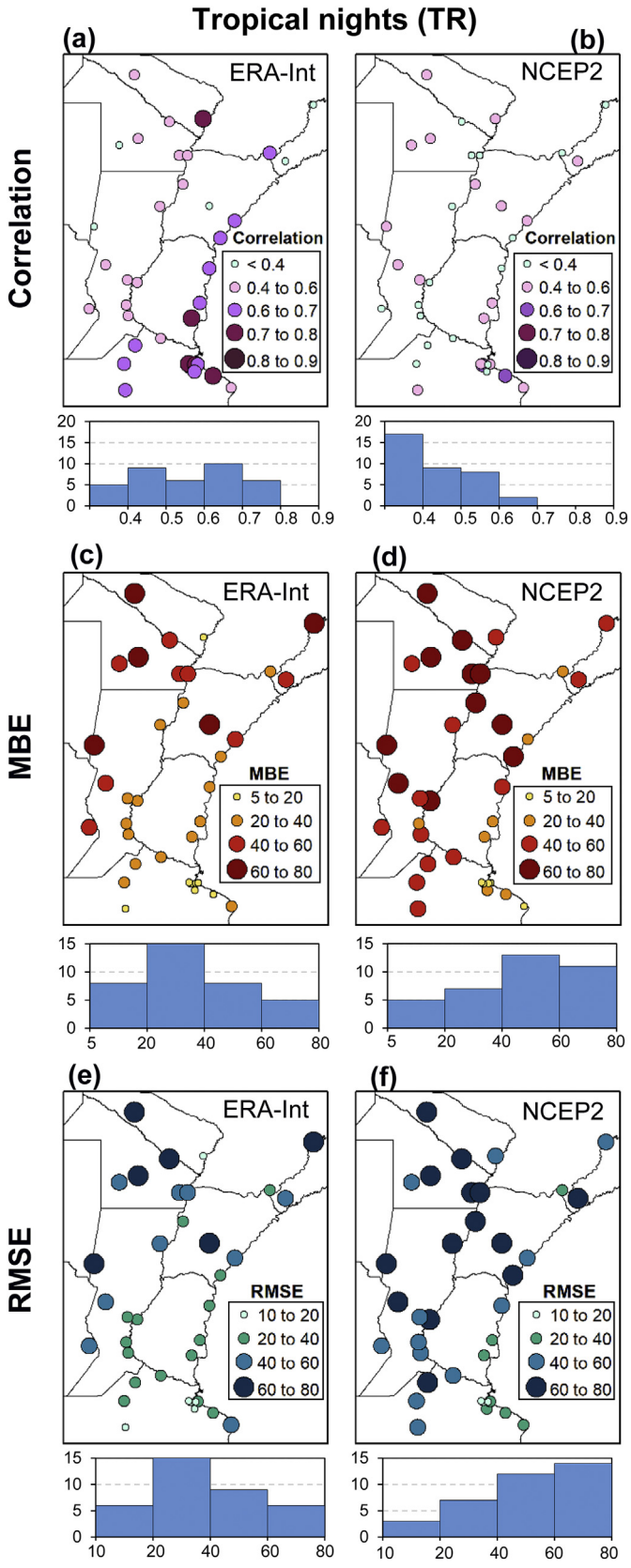

Fig. 8. Spatial distribution of the correlation coefficients (a, b), the MBE (c, d) and the RMSE (e, f) for tropical nights represented by the ERA-Interim and NCEP2 reanalyses for the period 1979–2011. Histograms are provided below of each map.

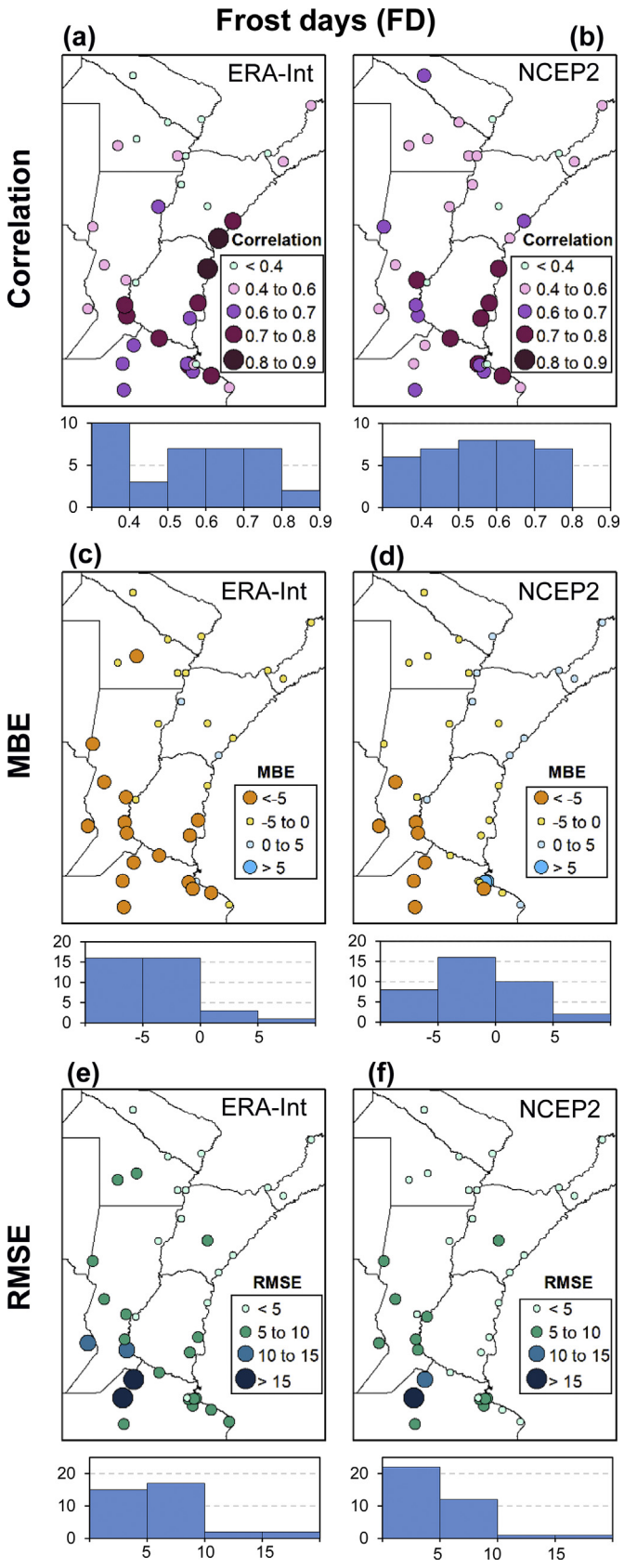

Fig. 9. Spatial distribution of the correlation coefficients (a, b), the MBE (c, d) and the RMSE (e, f) for frost days represented by the ERA-Interim and NCEP2 reanalyses for the period 1979–2011. Histograms are provided below of each map.

d). This underestimation represent almost 30% of the annual mean values of frost days towards the colder south, where both reanalyses exhibit the highest RMSE values (Fig. 9f and g).

5. Precipitation-related climate extremes

5.1. Intense precipitation events

We characterize the intensity of precipitation-related climate extremes using two indices (see Table 2): the annual maximum 1-day precipitation (RX1day) and the simple daily intensity index (SDII) for precipitation, which is the average accumulated precipitation in rainy days. [The RX5day was also studied, but is not shown due to its similarity to RX1day.]

The spatial distribution of RX1day (Fig. 10a) has a spatial gradient increasing from the southwest to the northeast that agrees with the annual mean precipitation fields (Fig. 1f). The climatological values in Fig. 10a of RX1day range from 75 mm to 120 mm. The area-averaged evolution of RX1day in Fig. 10b indicates that maximum 1-day precipitation events have increased from 1970 to about 2000, declining slightly since mid-2000s. Note the large dispersion in the time series of all stations (thin lines) that suggests a large spatial and temporal variability in intense precipitation events. Particularly, NEA exhibits high interannual variability in intense precipitation events as shown by the area-averaged time series of RX1day in Fig. 10b. The more intense events tend to occur during El Niño years (e.g., 1998, 2002). Precipitation events during La Niña years (e.g., 1989, 2008) do not achieve the same intensity. Table 4 presents ENSO-range periodicities for RX1day (a cycle of 3.6 years accounting for 27% of its variance) and for RX5day (a noticeable 2.5-yr mode that explains 35% of the total index variance). According to Fig. 10c, the annual maximum 1-day precipitation amounts present no definite pattern of change, perhaps due to the fact that precipitation is highly variable in this region.

The simple daily intensity index presents the highest values in the wettest portion of NEA, i.e. towards northeast (Fig. 10d). Although the SSA method does not extract trends with statistical significance for the area-averaged SDII time series (Fig. 10e), the 10-yr moving averages series shows that precipitation intensity has increased since the early 1970s to the present. Consistently, Fig. 10f indicates that the increase occurred in the whole region, with 31 out of 36 stations showing positive trends (11 of them significant at least at a 95% confidence level). The average change is about 1 mm/day in the last 50 years (see the time series of the area-averaged 10-yr moving average in Fig. 10e), with some areas showing increases of up to 1 mm/day per decade (see Fig. 10f). As in the case of RX1day index, the high dispersion in the 10-yr moving averages time series of all stations (Fig. 10e) indicates that the changes in precipitation intensity are modulated by large spatio-temporal variability. In particular, Table 4 shows that SDII is strongly influenced by an interannual variability cycle of 5 years that explains 35% of its variance.

5.2. Duration of wet and dry spells

Fig. 11 presents the maximum annual duration of dry and wet spells as characterized by the consecutive dry/wet days indices (CDD and CWD; see Table 2 for definitions). It is noted that wet spells refer to precipitation events and do not consider hydrological aspects (longer term flooding) due to recurring non-consecutive wet spells.

The climatology in Fig. 11a reveals a longitudinal spatial gradient ranging from 20 to 30 consecutive dry days in the east and increasing westwards to almost 50 days. This spatial gradient agrees with the precipitation climatology field (see Fig. 1f). Fig. 11b and c indicate that dry spell duration has increased in recent decades. Fig. 11b shows a continuous increase of dry spell duration over the whole region since the 1970s (see the time series of the area-averaged 10-yr moving average), also influenced by a high interannual variability. Fig. 11c

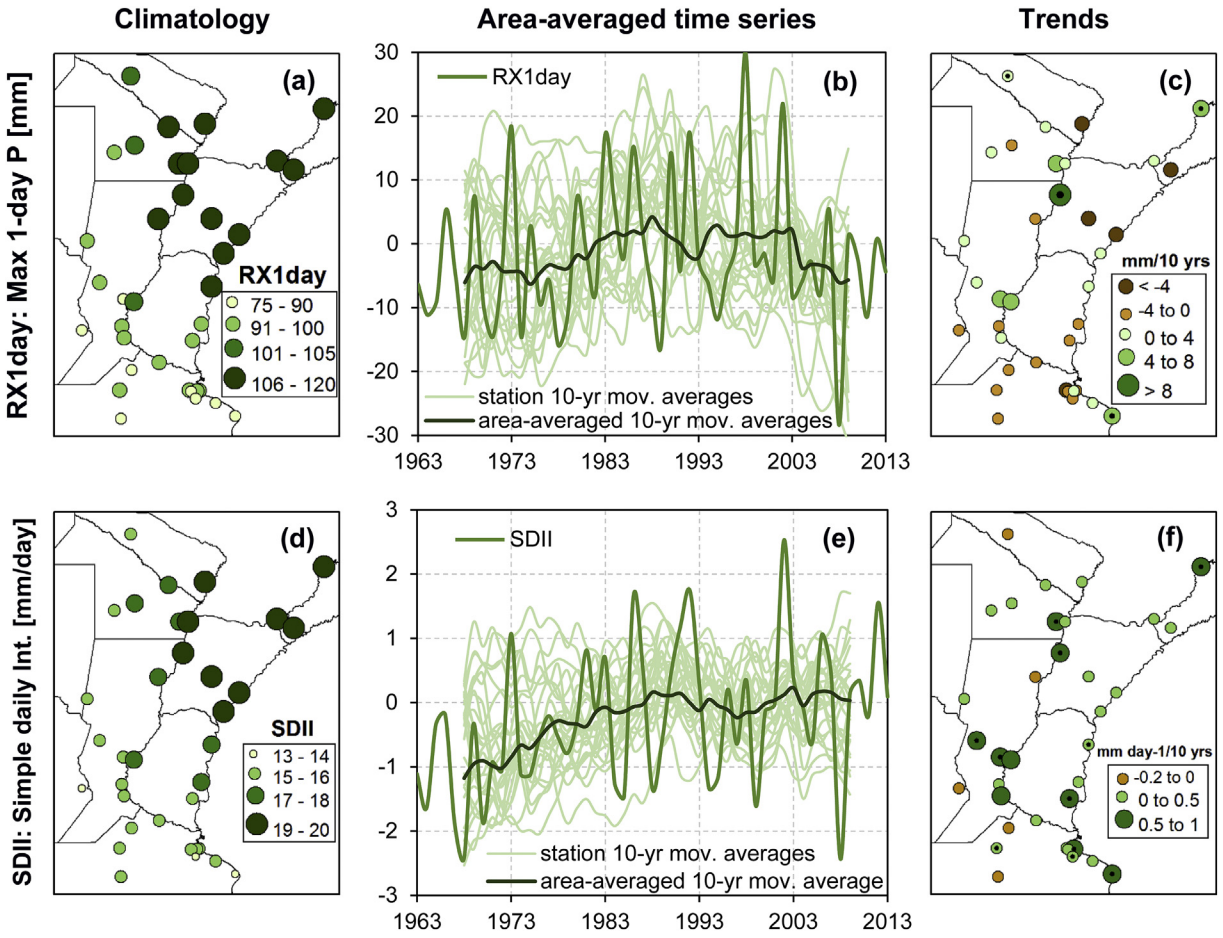

Fig. 10. Intense precipitation climate extremes characterized by the annual maximum 1-day precipitation amount (RX1day; a-c) and the simple daily intensity index (SDII, d-f). Left panels (a, d): climatological mean values in the 1963–2013 period. Middle panels (b, e): the temporal evolution of the anomalies of the area-averaged indices and their trends. Right panels (c, f): the spatial distribution of linear trends. Green colors indicate a shift towards wetter conditions wile brown colors towards drier conditions. Station highlighted with a black dot indicate a significant linear trend, at least at the 95% confidence level. The definition of each index is given in Table 2. The units of each index is shown in brackets. (For interpretation of the references to colour in this figure legend, the reader is referred to the web version of this article.)

shows a homogeneous pattern of change with 27 stations with positive trends (75% of the total observed stations) increasing the duration of dry spells by 1 to 5 dry days per decade. Notably, the largest increases occurred towards the north, where 5 locations have positive trends that exceed the confidence level of 95%.

Characteristics of the wet spells presented in Fig. 11d-e show that their duration is shorter than for dry spells: wet spells tend to last 4 to 5 days in most of the study region, although up to 7 consecutive wet days can occur towards the rainiest northeastern sector (Fig. 11d). Fig. 11e shows high interannual variability of wet spell anomalies with no noticeable trend. As seen in Fig. 11f, the spatial pattern of trends lacks adequate information, with few non-significant trends and the rest having no changes (and thus not plotted).

5.3. Precipitation-related extremes in reanalyses

The ability of the global reanalyses to represent precipitation-related extremes is evaluated for the annual maximum consecutive 5-day precipitation amount (RX5day) and the maximum annual number of consecutive dry days (CDD). RX5day is similar to RX1day discussed in Section 5.1, with the only difference that it considers amounts in five days instead of one, thus allowing for more stable results.

5.3.1. Maximum 5-day precipitation amount (RX5day)

According to Fig. 12a, the observed climatology of RX5day (circles) presents a southwest-northeast gradient that ranges from 125 mm to 200 mm with high spatial variability. Both reanalysis climatologies

Table 4
Summary of the main variability modes of precipitation-related extremes found with SSA.

SSA results of precipitation-based indices					
	Index	Index name	Components	Trend or dominant period (year/cycle)	Explained variance (%)
Intensity	RX1day	Max 1-day precipitation	T-PC1 and T-PC2	3.6	27
	RX5day	Max 5-day precipitation	T-PC1 and T-PC2	2.5	35
	SDII	Simple daily intensity index	T-PC1 and T-PC2	5	35
Duration	CWD	Consecutive wet days	No significant modes		
	CDD	Consecutive dry days	No significant modes		

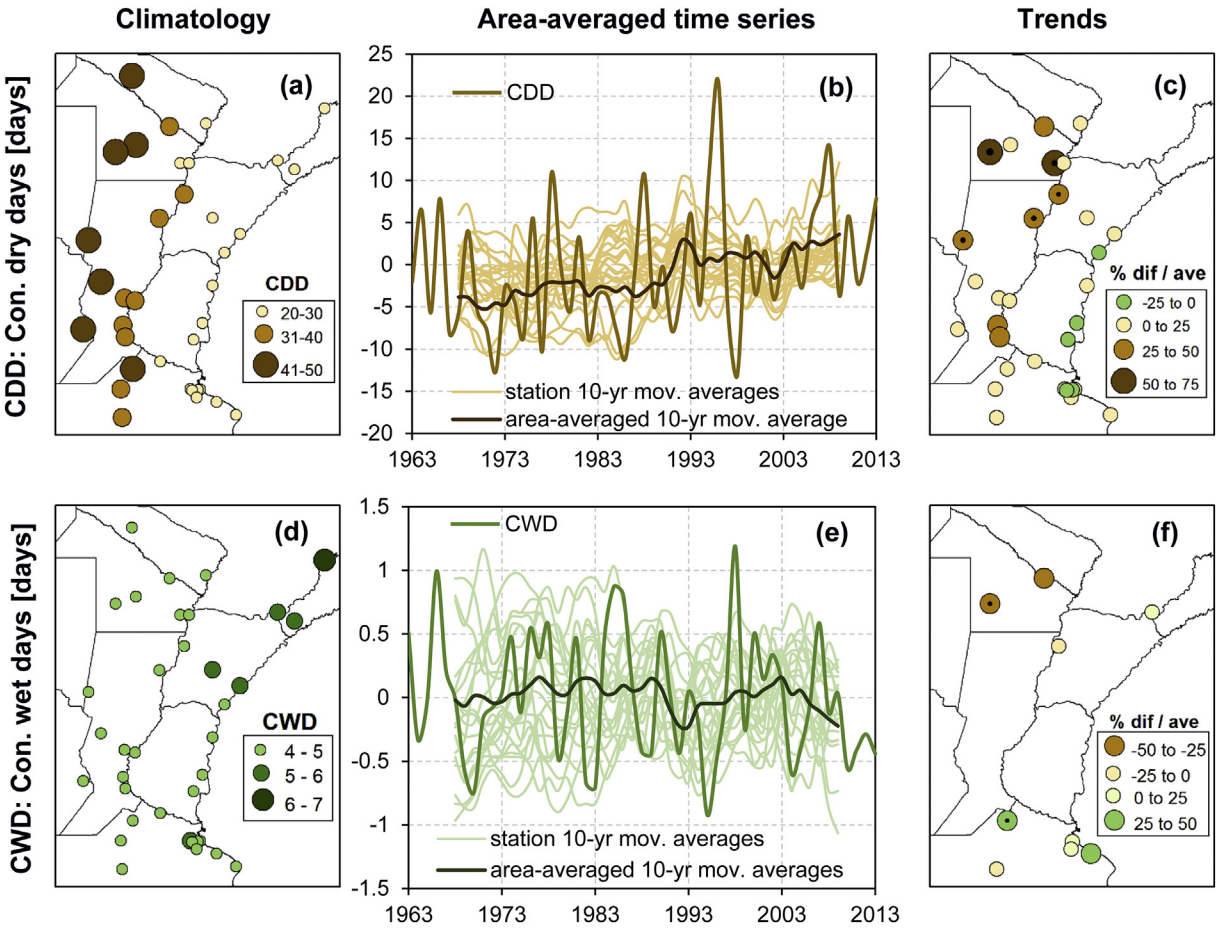

Fig. 11. Duration of wet and dry spells characterized by the annual consecutive dry days (CDD; a-c) and the consecutive wet days (CWD, d-f). Left panels (a, d): climatological mean values in the 1963–2013 period. Middle panels (b, e): the temporal evolution of the anomalies of the area-averaged indices and their trends. Right panels (c, f): the spatial distribution of linear trends computed in percentage units as the ratio between the linear trend in the 51 years analyzed and the temporal average in the same period for each station. Green colors indicate a shift towards wetter conditions wile brown colors towards drier conditions. Station highlighted with a black dot indicate a significant linear trend, at least at the 95% confidence level. The definition of each index is given in Table 2. The units of each index is shown in brackets. (For interpretation of the references to colour in this figure legend, the reader is referred to the web version of this article.)

depict a smoothed version of the observed spatial variability. However, the reanalyses reproduce the temporal variability of the observed RX5day, achieving correlation coefficients close to 0.65. Yet, there are periods (1998–2000) in which large departures are found. The time series show that ERA-Interim and NCEP2 underestimate the time evolution of area-averaged RX5day by about 16–18 mm, which represents relative errors of about 10–12% with respect to the area-averaged observations.

Fig. 13 compares the spatial distribution of the RX5day for ERA-Interim and NCEP2 reanalyses against in-situ observations. Both reanalyses fail to represent the observed RX5day, as their correlations are lower than 0.2 in the whole region (Fig. 13a and b, respectively). The two reanalyses also present dry biases of more than 40 mm towards the north of the study region (Fig. 13c and d). The RMSE (Fig. 13e and f) are large throughout the study region, with more than 80% of the stations (30 out of 36) presenting RMSE values higher than 60 days (see histograms below the maps in Fig. 13e and f).

5.3.2. Consecutive dry days (CDD)

Fig. 12b shows that the observed climatology of CDD (circles) presents a strong east-west spatial gradient (discussed in Section 5.2). Both reanalysis climatologies also display the east-west gradient (shades) but the ERA-Interim underestimates the observed spatial variability while NCEP2 overestimates it. The area-averaged CDD time series have a similar evolution reaching correlation coefficients close to 0.7. Consistently with the spatial behavior, ERA-Interim underestimates the observed time variability with a mean bias error of 13 days (36% of the observed mean value in the whole period) while NCEP2 overestimates the temporal evolution of CDD reaching a mean bias error of 2 days, which represents a 6% of the observed mean value.

Fig. 14 presents the evaluation of the CDD metrics, and a comparison of Figs. 14 and 13 indicates that both reanalyses performs better for CDD than for RX5day. ERA-Interim reproduces the observed CDD with higher correlations than NCEP2, mainly towards the northern sector (Fig. 14a and b). As shown by Fig. 14c-f, both reanalyses present the highest biases towards the driest east: RMSE acquires values higher than 20 days (Fig. 14e and f) but while ERA-Interim underestimates observations (Fig. 14c), NCEP2 overestimates them (Fig. 14d). The histograms in Fig. 14c and d show that ERA-Interim acquires frequent mean bias in the range $-20 < MBE < -10$ while NCEP2 most frequent errors are in the range $0 > MBE > 10$, suggesting that the ERA-Interim underestimation is higher than the NCEP2 overestimation.

6. Discussion

6.1. Changes in extreme events and potential impacts

The results show that minimum-temperature extremes had a clear signal of nighttime warming due to a significant increase in warm nights and a concurrent significant decrease in cold nights. Maximum-

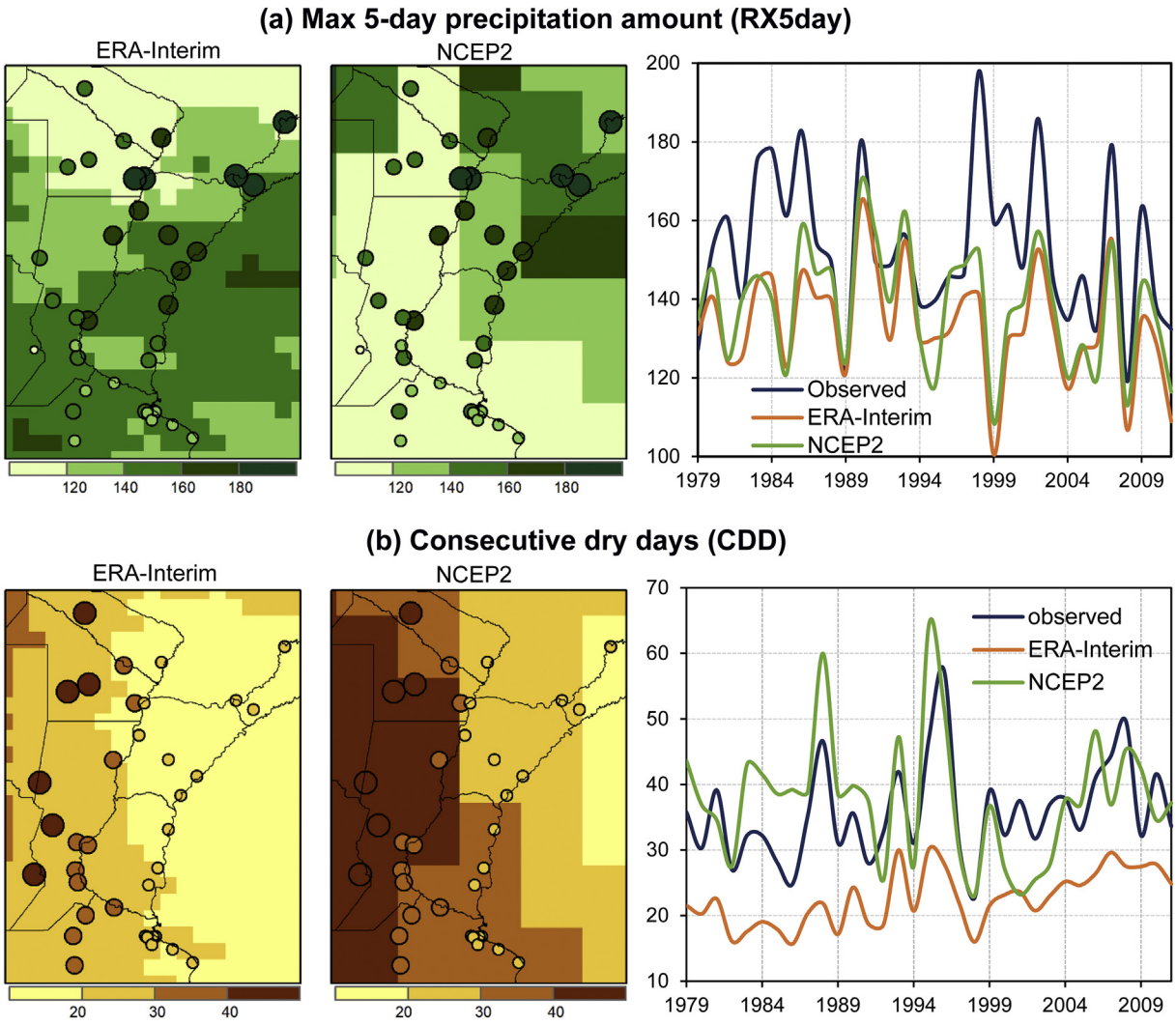

Fig. 12. Intense precipitation events characterized by the annual maximum 5-day precipitation amount (RX5day, a) and short-term droughts represented by the annual maximum consecutive dry days (CDD, b) represented by the ERA-interim and NCEP2 reanalyses for the period 1979–2011 and compared with observations. Spatial distribution of mean climatology values are given in the first two panels while area-averaged time series in the third panel of each row.

temperature extremes also exhibited a daytime warming resulting from a significant increase in warm days and a significant decrease in cold days. While the minimum temperature warming seems to have been stabilizing in recent decades, the maximum temperature warming continues to rise. According to literature, these changes may have agricultural implications as the decrease in cold nights shortens crops' critical growth periods reducing wheat and barley yields (Magrin et al., 2009; García et al., 2015). On the other hand, the increase of warm days affect the critical growth periods of maize and sunflower in summer, while the decrease of cold days may reduce the flowering and yield of winter wheat (Magrin et al., 2012).

The results also suggest that the region is experiencing longer and more frequent warm spells than cold spells. The longer duration of heat waves may have important impacts on the population, increasing their mortality risk by heat strokes and producing more frequent collapses of energy systems (Magrin et al., 2014). In agriculture, the yields of maize and sunflower can be reduced because their critical periods are very sensitive to the summer high temperatures (Rondanini et al., 2006; Mayer et al., 2012).

The increased intensity of heavy precipitation events in the last decades over the whole NEA constitutes a growing risk for urban settlements where heavy rainfall may exceed the capacity of drainage systems, causing significant infrastructure losses and, in the most extreme cases, deaths (Barros et al., 2015; Lovino, 2015). Intense precipitation events in the predominantly flat agricultural plains lead to extensive waterlogging with important economic impacts due to loss of crops and decreased livestock productivity. While precipitation has increased, dry spells in recent decades have tended to last longer, suggesting that more persistent short-term droughts may affect agriculture activities, mainly in the drier area towards the northwest.

6.2. Large-scale climate factors and the changes and variability in NEA climate extremes

The South American climate underwent a transition in the 1970s, linked to the 1976–77 global climate shift, which strongly affected the South American Monsoon System (Carvalho et al., 2011). It has been speculated that several large-scale climate-forcing factors could have combined to cause this change, including a cold-to-warm sea surface temperature shift in the tropical Pacific Ocean (Huang et al., 2005; Jacques-Coper and Garreaud, 2015) and a multidecadal cooling in the tropical Atlantic Ocean (Seager et al., 2010; Barreiro et al., 2014). This climate shift appears to have been a source of change for trends and variability in precipitation, river streamflow and temperature in several regions of South America (e.g., Marengo, 2004; Kayano et al., 2009; Castino et al., 2016). Agosta and Compagnucci (2008) reported that the

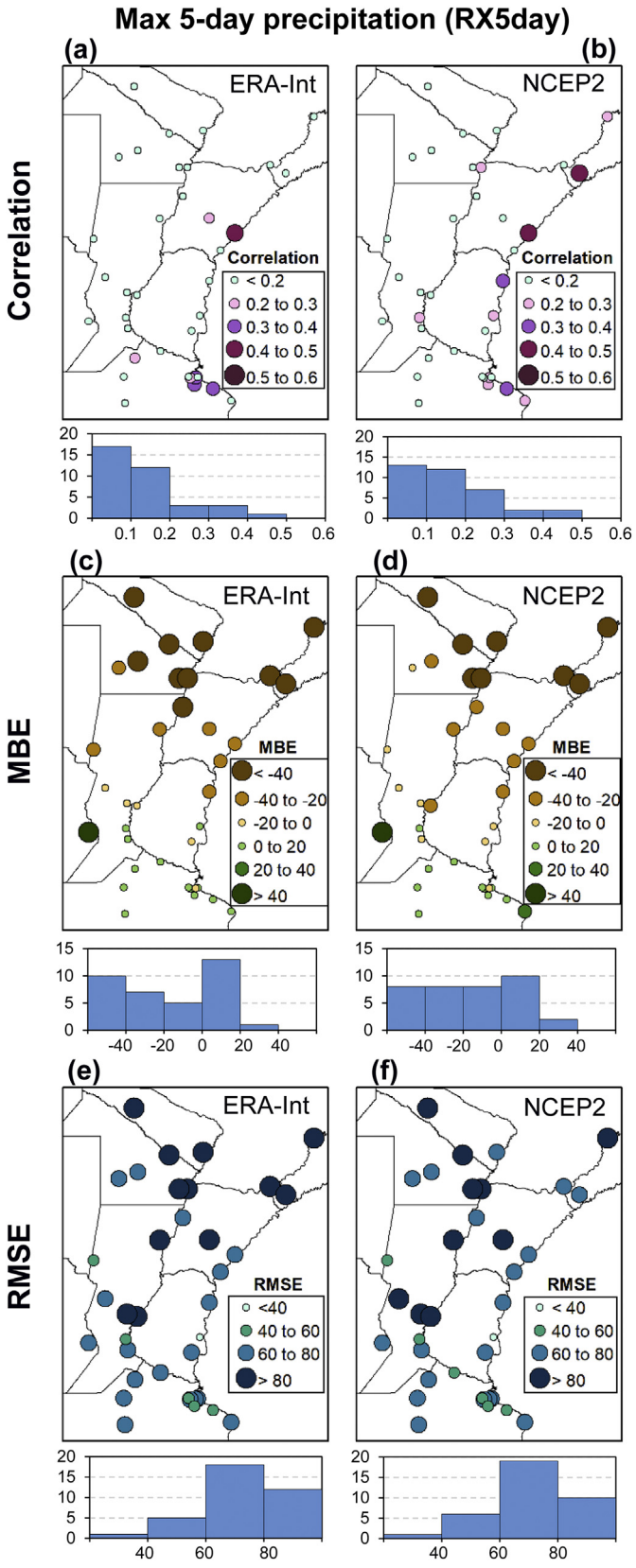

Fig. 13. Spatial distribution of the correlation coefficients, the MBE and the RMSE for maximum 5-day precipitation (RX5day) represented by the ERA-Interim and NCEP2 reanalyses for the period 1979–2011. Histograms are provided below of each map.

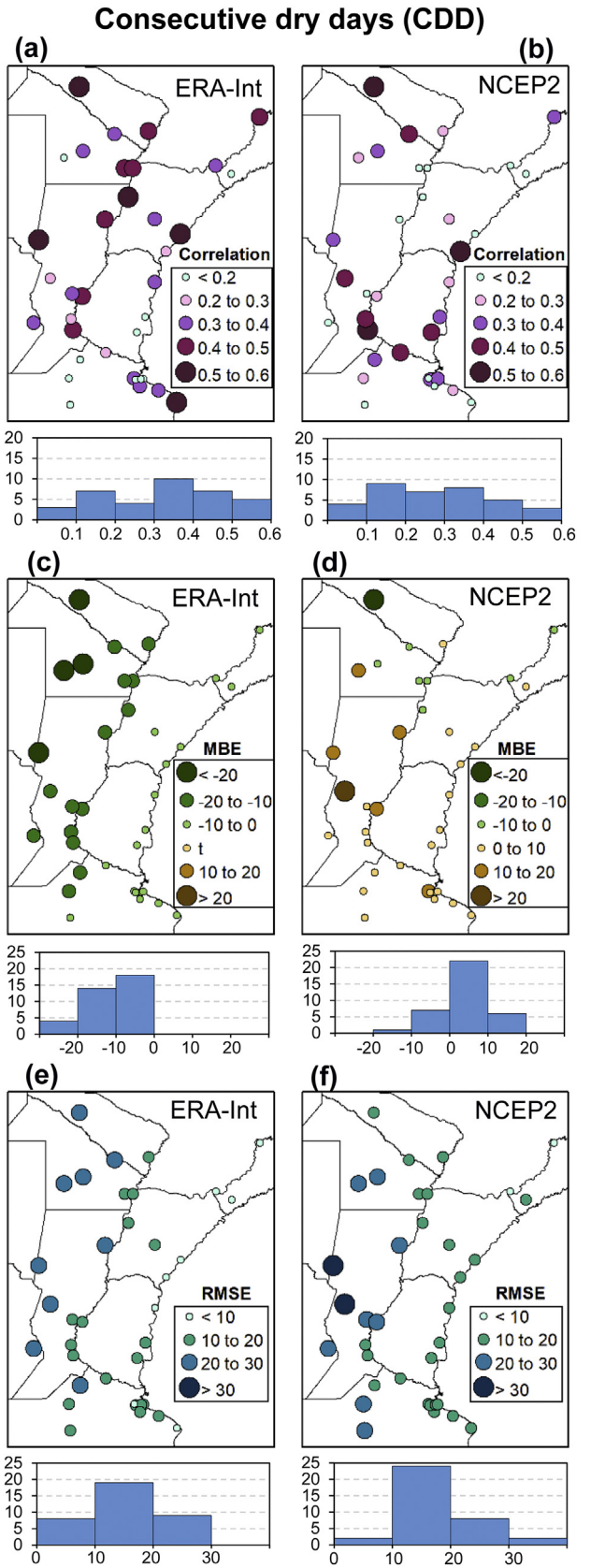

Fig. 14. Spatial distribution of the correlation coefficients, the MBE and the RMSE for the annual maximum consecutive dry days (CDD) represented by the ERA-Interim and NCEP2 reanalyses for the period 1979–2011. Histograms are provided below of each map.

wetter conditions could have been influenced by the 1976–1977 climate shift that reduced the cyclonic activity at mid-latitudes together with a stronger northerly flow, which brings in higher humidity levels from northeastern Argentina. In this context, our results suggesting that intense precipitation events and minimum temperature extremes experienced long-term increases since the 1970s in northeastern Argentina, are in agreement with Cavalcanti et al. (2015) and Carril et al. (2016).

Extremes of minimum temperature (cold and warm nights) showed a stabilization in their trends since the 1980s. Rusticucci et al. (2016) proposed that these trends could be influenced by a shift towards the west of the South Atlantic anticyclone together with an increase in the north component of the wind measured by the meridional wind at 925 hPa in central Argentina that occurred during 1970s and 1980s being stabilized during the 1990s and 2000s.

Other changes seem to have occurred since the 2000s. This study shows that some of the observed increases in precipitation and minimum temperature extremes seem to have stabilized in recent decades in northeastern Argentina. We showed that the magnitude of intense precipitation events appears to be stabilizing in the last decade or so. The stabilization of the long-term wetting trend has been discussed in recent years (e.g., Seager et al., 2010; Barreiro et al., 2014; Lovino et al., 2014). These authors suggested that a cold phase of the Atlantic Multidecadal Oscillation (AMO) may have favored wet anomalies in decadal time scales between 1970s and 2000s over NEA while the reversal in the wetting trend could be associated to a shifting towards a warm phase of the AMO (Li et al., 2018) that may have forced a long-term decrease in precipitation during the late 2000s.

Our results suggest that the interannual variability significantly affects minimum-temperature and intense precipitation extremes in northeastern Argentina (in agreement with Rusticucci, 2012 and Carril et al., 2016). Interestingly, minimum-temperature extremes (including frost days) showed a significant interannual cycle of 4 years. Recently, Lovino et al. (2018) found that regional minimum temperature can be related to ENSO with a periodicity of roughly 4 years. It is well known that the number of frost days in northeastern Argentina is highly influenced by the ENSO phenomenon: less frost days are observed during El Niño years and more are found during La Niña years (Müller et al., 2000; Müller et al., 2003). In consonance with that, our results suggest that nighttime temperature extreme events might be also affected by the ENSO in this frequency. There is much evidence that ENSO modulates the interannual variability of extreme precipitation events over northeastern Argentina (e.g., Haylock et al., 2006; Grimm and Tedeschi, 2009; Cavalcanti, 2012). Our results suggest that extreme values of the area-averaged time series of RX1day and RX5day are associated to ENSO conditions. Consistently, the main significant periodicities of the intense precipitation events of one day and five days (3.6 and 2.5 years) found in this study were also reported in the ENSO SST pattern (Moron et al., 1998; Lovino et al., 2018) and ENSO indices (e.g., Wolter and Timlin, 2011).

6.3. The skill of NCEP2 and ERA-Interim reanalyses to represent NEA climate extremes

The ERA-Interim is a newer reanalysis that unlike the older NCEP2 includes assimilation of surface temperature observations. Our findings are in line with this information, as they show that ERA-Interim exhibits greater ability to reproduce the spatial and temporal variability of summer days than NCEP2 over the study region. NCEP2 and ERA-Interim tend to represent maximum-temperature extremes (here characterized by summer days) better than minimum-temperature extremes (as represented by tropical nights and frost days). This result is consistent with Rusticucci and Kousky (2002) and Zaninelli et al. (2015) who showed similar differences between NCEP and ERA40. Both reanalyses represent the interannual variability of tropical nights and frost days, although with significant positive systematic errors for tropical nights even for the ERA-Interim that assimilates observed temperature. Still, NCEP2 fails to reproduce the spatial patterns of both summer days and tropical nights and both reanalysis have closer values among themselves than with observations. Frost days exhibit negative mean bias errors, which intriguingly are larger for ERA-Interim. In summary, while the reanalyses can reproduce the interannual variability of temperature-related climate extremes, magnitudes are off, particularly for tropical nights.

Precipitation-related extreme events are more difficult to reproduce by reanalysis products. The two reanalyses were able to recognize the time evolution of area-averaged intense precipitation events in the last decades, but smooth out the spatial distribution of these events. The RX5day is represented with significant dry biases towards the north of the study region. These results agree with Boers et al. (2015), who reported that ERA-Interim fail to reproduce large convective systems in southeastern South America, and Silva et al. (2011) and Albuquerque de Almeida et al. (2018), who found that NCEP2 presents dry biases and difficulties to simulate the intensity of precipitation. The two reanalyses recognized dry spells patterns as characterized by CDD, although NCEP2 tends to represent longer dry spells, and ERA-Interim shorter dry spells compared to observations. Thus, our results suggest that reanalyses products have limits that should be taken carefully into account if they are included in studies that involve changes in climate extremes in northeastern Argentina, particularly for precipitation-related extremes.

7. Concluding remarks

This paper has investigated the variability and changes in daily climate extreme events during the last five decades in the fertile northeast region of Argentina. The extremes include warm and cold days and nights, temperature diurnal amplitude, frost days, heat and cold waves, intense precipitation events and dry and wet spells. The intensity, duration and frequency of temperature- and precipitation-related climate extremes were studied using 15 indices of the core set of ETCCDI indices, selected according to their capacity to represent relevant extreme events in the study region. We also assessed the ability of the ERA-Interim and NCEP2 reanalyses to reproduce the observed variability of climate extremes during the period 1979–2011.

The changes in daily temperature extremes reveal a trend towards warmer conditions over northeastern Argentina, which is consistent with what has been observed in other regions of the world (e.g., Seneviratne et al., 2012; Donat et al., 2013). This warming is revealed as an increase of warm days and warm nights, as well as a decrease of cold days and cold nights. Although the number of cold nights declined following the general warming trend in the region, the number has not changed significantly since 1980. The number of frost days exhibits large interannual and decadal variability without noticeable trends. The diurnal amplitude of temperature in winter has been increasing since about 2000, possibly as a result of the decrease in cold days, i.e., those days with maximum temperature lesser than the 10th percentile, and despite the lack of changes in the number of cold nights.

Heat and cold waves also reflect the general warming in NEA. Firstly, heat waves almost double the frequency and duration of cold waves. Second, during recent decades heat waves have tended to increase their duration and cold waves tended to be less persistent in time. The occurrence of longer heat waves is also related to changes in precipitation features noted in the trend towards longer dry spells. These results agree with Seneviratne et al. (2012) who showed that the longer persistence of dry days during warm seasons contributes to higher temperatures and more extended duration of heat waves. Our results showed that heat waves are more frequent and persistent towards the west, where dry spells persist longer, with events reaching up to 50 days without rain.

Daily precipitation intensities in the range of 13–20 mm day^{-1} are common in NEA. However, in occasions, extreme precipitation events

can exceed 100 mm in one day and 200 mm in five days, particularly towards the wetter northeast. Our results show that intense precipitation events are highly influenced by interannual variability and, although no significant trends have been found with the SSA method, a steady increase of mean intensity values occurred since 1970. Since the region is mostly flat and has several important rivers, the increased intensity of extreme precipitation events has led to severe floods affecting agriculture and human settlements. The annual maximum amount of 1-day and 5-day precipitation events also increased since 1970, although it seems to be stabilizing in recent years, as discussed above. The observed high variability is influenced by frequent and intense mesoscale convective systems and convective storms (Zipser et al., 2006; Rasmussen et al., 2016) that cause extreme precipitation events everywhere in the region. The prevalence for few days of convective systems and convective storms also explains the short duration of consecutive wet days. Wet spells do not persist for more than 5–6 days in average. However, during those days large amounts of precipitation can accumulate leading to severe floods (Cavalcanti, 2012).

Finally, the ERA-Interim and NCEP2 reanalyses have different degrees of success in representing the observed extreme temperature and precipitation events. ERA-Interim can recognize the evolution of temperature extremes as number of summer days and tropical nights in time and space although with biases in magnitude. NCEP2 has a similar behavior for the area-averaged time evolution, but poor correlations are found at individual stations.

The two reanalyses represent extreme precipitation events with large biases, which are particularly noticeable when looking at the performance locally at each station. Although both reanalyses tend to recognize the variability of the area-averaged annual 5-day maximum precipitation in time, they underestimate the representation of their spatial distribution, mainly in the wetter northeast. Despite the large biases, the two reanalyses can represent better the short-term drought characterized by the annual maximum consecutive dry days than the extreme precipitation events represented by annual 5-day maximum precipitation. In general, reanalyses perform better for temperature extremes than for precipitation extremes. Although reanalyses would be expected to add information for climate extremes in areas of scarce observations like northeastern Argentina, they still need to be used with great caution and as a complement to observations.

Acknowledgements

We are grateful to the anonymous reviewers whose constructive comments and recommendations helped to improve the manuscript. This research was carried out with support of Projects CRN3035 and CRN3095 of the Inter-American Institute for Global Change Research (IAI), which is supported by the US National Science Foundation. NOAA Grant NA14NES4320003 and a UNL Project C.A.I. + D. 2011 35/180 are also acknowledged. Miguel Lovino and Omar Müller were supported by fellowships from CONICET, Argentina. The NCEP2 climate indices were provided by the Canadian Centre for Climate Modelling and Analysis from the archive website http://www.cccma.ec.gc.ca/data/climdex/ (Sillmann et al., 2013).

References

Agosta, E.A., Compagnucci, R.H., 2008. The 1976/77 austral summer climate transition effects on the atmospheric circulation and climate in southern South America. J. Clim. 21, 4365–4383. http://dx.doi.org/10.1175/2008JCLI2137.1.

Albuquerque de Almeida, V., Marton, E., Nunes, A.M.B., 2018. Assessing the ability of three global reanalysis products to reproduce South American monsoon precipitation. Atmósfera 31 (1), 1–10. http://dx.doi.org/10.20937/ATM.2018.31.01.01.

Alexander, L.V., Zhang, X., Peterson, T.C., Caesar, J., Gleason, B., Klein Tank, A.M., Haylock, M., Collins, D., Trewin, B., Rahimzadeh, F., Tagipour, A., Rupa Kumar, K., Revadekar, J., Griffiths, G., Vincent, L., Stephenson, D.B., Burn, J., Aguilar, E., Brunet, M., Taylor, M., New, M., Zhai, P., Rusticucci, M., Vazquez-Aguirre, J.L., 2006. Global observed changes in daily climate extremes of temperature and precipitation. J. Geophys. Res.-Atmos. 111, D05109. http://dx.doi.org/10.1029/2005JD006290.

Allen, M.R., Smith, L.A., 1996. Monte Carlo SSA: detecting irregular oscillations in the presence of colored noise. J. Climate 9, 3373–3404. http://dx.doi.org/10.1175/1520-0442(1996)009<3373:MCSDIO>2.0.CO;2.

Barreiro, M., Diaz, N., Renom, M., 2014. Role of the global oceans and land–atmosphere interaction on summertime interdecadal variability over northern Argentina. Clim. Dyn. 42, 1733–1753. http://dx.doi.org/10.1007/s00382-014-2088-6.

Barros, V.R., Boninsegna, J.A., Camilloni, I.A., Chidiak, M., Magrín, G.O., Rusticucci, M., 2015. Climate change in Argentina: trends, projections, impacts and adaptation. WIREs Clim. Change 6, 151–169. http://dx.doi.org/10.1002/wcc.316.

Barrucand, M., Rusticucci, M., Vargas, W., 2008. Temperature extremes in the south of South America in relation to Atlantic Ocean surface temperature and southern hemisphere circulation. J. Geophys. Res. 113, D20111. http://dx.doi.org/10.1029/2007JD009026.

Berbery, E.H., Barros, V.R., 2002. The hydrologic cycle of the La Plata basin in South America. J. Hydrometeorol. 3 (6), 630–645. http://dx.doi.org/10.1175/1525-7541(2002)003<0630:THCOTL>2.0.CO;2.

Berbery, E.H., Collini, E.A., 2000. Springtime precipitation and water vapor flux over southeastern South America. Mon. Weather Rev. 128, 1328–1346.

Boers, N., Bookhagen, B., Marengo, J., Marwan, N., von Storch, J., Kurths, J., 2015. Extreme rainfall of the south American monsoon system: a dataset comparison using complex networks. J. Clim. 28, 1031–1056. http://dx.doi.org/10.1175/JCLI-D-14-00340.1.

Bronaugh, D., Werner, A., 2013. Zhang + Yue- Pilon Trends Package, Package "Zyp" Version 0.10-1. License LGPL-2.1 URL. http://r-project.og.

Carbajo, A.E., Cardo, M.V., Vezzani, D., 2012. Is temperature the main cause of dengue rise in non-endemic countries? The case of Argentina. Int. J. Health Geogr. 11, 26. http://dx.doi.org/10.1186/1476-072X-11-26.

Carril, A.F., Cavalcanti, I.F.A., Menéndez, C.G., Sörensson, A., López-Franca, N., Rivera, J., Robledo, F., Zaninelli, P., Ambrizzi, T., Penalba, O., da Rocha, R., Sánchez, E., Bettolli, M., Pessacg, N., Renom, M., Ruscica, R., Solman, S., Tencer, B., Grimm, A., Rusticucci, M., Cherchi, A., Tedeschi, R., Zamboni, L., 2016. Extreme events in the La Plata basin: a retrospective analysis of what we have learned during CLARIS-LPB project. Clim. Res. 68, 95–116. http://dx.doi.org/10.3354/cr01374.

Carvalho, L.M.V., Cavalcanti, I.F.A., 2016. The South American Monsoon System (SAMS). In: de Carvalho, L., Jones, C. (Eds.), The Monsoons and Climate Change. Springer Climate. Springer, Cham. http://dx.doi.org/10.1007/978-3-319-21650-8_6.

Carvalho, L.M.V., Jones, C., Silva, A.E., Liebmann, B., Silva Dias, P.L., 2011. The south American monsoon system and the 1970s climate transition. Int. J. Climatol. 31, 1248–1256. http://dx.doi.org/10.1002/joc.2147.

Castino, F., Bookhagen, B., Strecker, M.R., 2016. River-discharge dynamics in the southern Central Andes and the 1976–77 global climate shift. Geophys. Res. Lett. 43. http://dx.doi.org/10.1002/2016GL070868.

Cavalcanti, I.F.A., 2012. Large scale and synoptic features associated with extreme precipitation over South America: a review and case studies for the first decade of the 21st century. Atmos. Res. 118, 27–40. http://dx.doi.org/10.1016/j.atmosres.2012.06.012.

Cavalcanti, I.F.A., Carril, A.F., Penalba, O.C., Grimm, A.M., Menéndez, C.G., Sanchez, E., Chechi, A., Sörensson, A., Robledo, F., Rivera, J., Pántano, V., Betolli, L.M., Zaninelli, P., Zamboni, L., Tedeschi, R.G., Dominguez, M., Ruscica, R., Flach, R., 2015. Precipitation extremes over La Plata Basin—review and new results from observations and climate simulations. J. Hydrol. 523, 211–230. http://dx.doi.org/10.1016/j.jhydrol.2015.01.028.

CCSP, 2008. Weather and climate extremes in a changing climate. Regions of focus: North America, Hawaii, Caribbean, and U.S. Pacific Islands. In: Karl, Thomas R., Meehl, Gerald A., Miller, Christopher D., Hassol, Susan J., Waple, Anne M., Murray, William L. (Eds.), A Report by the U.S. Climate Change Science Program and the Subcommittee on Global Change Research. Department of Commerce, NOAA's National Climatic Data Center, Washington, D.C., USA (164 pp).

Dee, D.P., Uppala, S.M., Simmons, A.J., Berrisford, P., Poli, P., Kobayashi, S., Andrae, U., Balmaseda, M.A., Balsamo, G., Bauer, P., Bechtold, P., Beljaars, A.C.M., van de Berg, L., Bidlot, J., Bormann, N., Delsol, C., Dragani, R., Fuentes, M., Geer, A.J., Haimberger, L., Healy, S.B., Hersbach, H., Hólm, E.V., Isaksen, L., Kållberg, P., Köhler, M., Matricardi, M., Mcnally, A.P., Monge-Sanz, B.M., Morcrette, J.-J., Park, B.-K., Peubey, C., de Rosnay, P., Tavolato, C., Thépaut, J.-N., Vitart, F., 2011. The ERA-interim reanalysis: configuration and performance of the data assimilation system. Q. J. R. Meteorol. Soc. 137, 553–597. http://dx.doi.org/10.1002/qj.828.

Déqué, M., 2012. Continuous variables. In: Jolliffe, I.T., Stephenson, D.V. (Eds.), Forecast Verification – A Practitioner's Guide in Atmospheric Science, 2nd ed. John Wiley and Sons, Chichester, UK, pp. 97–120.

Donat, M.G., Alexander, L., Yang, H., Durre, I., Vose, R., Caesar, J., 2013. Global land-based datasets for monitoring climatic extremes. Bull. Am. Meteorol. Soc. 94, 997–1006. http://dx.doi.org/10.1175/BAMS-D-12-00109.1.

ECLAC (Economic Commission for Latin America and the Caribbean), 2015. The Economics of Climate Change in Latin America and the Caribbean Paradoxes and Challenges of Sustainable Development. United Nations, Santiago, Chile. http://repositorio.cepal.org/bitstream/handle/11362/37311/S1420655_en.pdf.

Fernández-Long, M.E., Müller, G.V., Beltrán-Przekurat, A., Scarpati, O.E., 2013. Long-term and recent changes in temperature-based agroclimatic indices in Argentina. Int. J. Climatol. 33, 1673–1686. http://dx.doi.org/10.1002/joc.3541.

Field, C.B., Barros, V.R., Mach, K.J., Mastrandrea, M.D., van Aalst, M., Adger, W.N., Arent, D.J., Barnett, J., Betts, R., Bilir, T.E., Birkmann, J., Carmin, J., Chadee, D.D., Challinor, A.J., Chatterjee, M., Cramer, W., Davidson, D.J., Estrada, Y.O., Gattuso, J.-P., Hijioka, Y., Hoegh-Guldberg, O., Huang, H.Q., Insarov, G.E., Jones, R.N., Kovats, R.S., Romero-Lankao, P., Larsen, J.N., Losada, I.J., Marengo, J.A., Mclean, R.F., Mearns, L.O., Mechler, R., Morton, J.F., Niang, I., Oki, T., Olwoch, J.M., Opondo, M.,

Poloczanska, E.S., Pörtner, H.-O., Redsteer, M.H., Reisinger, A., Revi, A., Schmidt, D.N., Shaw, M.R., Solecki, W., Stone, D.A., Stone, J.M.R., Strzepek, K.M., Suarez, A.G., Tschakert, P., Valentini, R., Vicuña, S., Villamizar, A., Vincent, K.E., Warren, R., White, L.L., Wilbanks, T.J., Wong, P.P., Yohe, G.W., 2014. Technical summary. In: Field, C.B., Barros, V.R., Dokken, D.J., Mach, K.J., Mastrandrea, M.D., Bilir, T.E., Chatterjee, M., Ebi, K.L., Estrada, Y.O., Genova, R.C., Girma, B., Kissel, E.S., Levy, A.N., MacCracken, S., Mastrandrea, P.R., White, L.L. (Eds.), Climate Change 2014: Impacts, Adaptation, and Vulnerability. Part A: Global and Sectoral Aspects. Contribution of Working Group II to the Fifth Assessment Report of the Intergovernmental Panel on Climate Change. Cambridge University Press, Cambridge, United Kingdom and New York, NY, USA, pp. 35–94.

García, G.A., Dreccer, M.F., Miralles, D.J., Serrago, R.A., 2015. High night temperatures during grain number determination reduce wheat and barley grain yield: a field study. Glob. Chang. Biol. 21 (11), 4153–4164. http://dx.doi.org/10.1111/gcb.13009.

Ghil, M., Vautard, R., 1991. Interdecadal oscillations and the warming trend in global temperature time series. Nature 350, 324–327. http://dx.doi.org/10.1038/350324a0.

Ghil, M., Allen, M., Dettinger, M.D., Ide, K., Kondrashov, D., Mann, M., Robertson, A., Saunders, A., Tian, Y., Varadi, F., Yiou, P., 2001. Advanced spectral method for climatic time series. Rev. Geophys. 40, 1–41. http://dx.doi.org/10.1029/2001RG000092.

Grimm, A.M., Tedeschi, R.G., 2009. ENSO and extreme rainfall events in South America. J. Clim. 22, 1589–1609. http://dx.doi.org/10.1175/2008JCLI2429.1.

Grimm, A.M., Laureanti, N.C., Rodakoviski, R.B., Gama, C.B., 2016. Interdecadal variability and extreme precipitation events in South America during the monsoon season. Clim. Res. 68, 277–294. http://dx.doi.org/10.3354/cr01375.

Guha-Sapir, D., Below, R., Hoyois, P., 2015. EM-DAT: International Disaster Database. Catholic University of Louvain, Brussels, Belgium.

Hardoy, J., Pandiella, G., 2009. Urban poverty and vulnerability to climate change in Latin America. Environ. Urban. 21 (1), 203–224. http://dx.doi.org/10.1177/0956247809103019.

Haylock, M.R., Peterson, T.C., Alves, L.M., Ambrizzi, T., Anunciação, Y.M.T., Baez, J., Barros, V.R., Berlato, M.A., Bidegain, M., Coronel, G., Corradi, V., Garcia, V.J., Grimm, A.M., Karoly, D., Marengo, J.A., Marino, M.B., Moncunill, D.F., Nechet, D., Quintana, J., Rebello, E., Rusticucci, M., Santos, J.L., Trebejo, I., Vincent, L.A., 2006. Trends in total and extreme south American rainfall in 1960–2000 and links with sea surface temperature. J. Clim. 19, 1490–1512. http://dx.doi.org/10.1175/JCLI3695.1.

Huang, H., Seager, R., Kushnir, Y., 2005. The 1976/77 transition in precipitation over the Americas and the influence of tropical SST. Clim. Dyn. 24, 721–740. http://dx.doi.org/10.1007/s00382-005-0015-6.

IPCC, 2012. Managing the risks of extreme events and disasters to advance climate change adaptation. In: Field, C., Barros, V. (Eds.), A Special Report of Working Groups I and II of the IPCC. Cambridge University Press, Cambridge, UK and New York, NY, USA (582 pp.).

Jacques-Coper, M., Garreaud, R.D., 2015. Characterization of the 1970s climate shift in South America. Int. J. Climatol. 35, 2164–2179. http://dx.doi.org/10.1002/joc.4120.

Jones, R.W., Renfrew, I.A., Orr, A.B., Webber, G.M., Holland, D.M., Lazzara, M.A., 2016. Evaluation of four global reanalysis products using in situ observations in the Amundsen Sea embayment, Antarctica. J. Geophys. Res. Atmos. 121. http://dx.doi.org/10.1002/2015JD024680.

Kanamitsu, M., Ebisuzaki, W., Woollen, J., Yang, S., Hnilo, J.J., Fiorino, M.M., Potter, G.L., 2002. NCEP–DOE AMIP-II reanalysis (R-2). Bull. Am. Meteorol. Soc. 83, 1631–1643. http://dx.doi.org/10.1175/BAMS-83-11-1631.

Kayano, M.T., Andreoli, R.V., 2007. Relation of south American summer rainfall interannual variations with the Pacific decadal oscillation. Int. J. Climatol. 27, 531–540. http://dx.doi.org/10.1002/joc.1417.

Kayano, M.T., Pestrelo De Oliveira, C., Andreoli, R.V., 2009. Interannual relations between south American rainfall and tropical sea surface temperature anomalies before and after 1976. Int. J. Climatol. 29, 1439–1448. http://dx.doi.org/10.1002/joc.1824.

Klein Tank, A.M.G., Zwiers, F.W., Zhang, X., 2009. Guidelines on Analysis of Extremes in a Changing Climate in Support of Informed Decisions for Adaptation. WMO-TD No. 1500/WCDMP-No. 72, Geneva (52 pp).

Kodama, Y.M., 1992. Large-scale common features of subtropical precipitation zones (the Baiu frontal zone, the SPCZ and SACZ). 1. Characteristics of subtropical frontal zones. J. Meteorol. Soc. Jpn. 70, 813–836. http://dx.doi.org/10.2151/jmsj1965.70.4_813.

Krepper, C., Garcia, N., 2004. Spatial and temporal structures of trends and interannual variability of precipitation over the La Plata Basin. Q. Int. 114, 11–21. http://dx.doi.org/10.1016/S1040-6182(03)00038-7.

Krepper, C.M., García, N.O., Jones, P.D., 2006. Paraguay river basin response to seasonal rainfall. Int. J. Climatol. 26, 1267–1278. http://dx.doi.org/10.1002/joc.1313.

Laing, A.G., Fritch, J.M., 2000. The large-scale environments of the global populations of mesoscale convective complexes. Mon. Weather Rev. 128, 2756–2776. http://dx.doi.org/10.1175/1520-0493(2000)128<2756:TLSEOT>2.0.CO;2.

Lenters, J.D., Cook, K.H., 1997. On the origin of the Bolivian high and related circulation features of the south American climate. J. Atmos. Sci. 54, 656–678. http://dx.doi.org/10.1175/1520-0469(1997)054<0656:OTOOTB>2.0.CO;2.

Li, F., Orsolini, Y.J., Wang, H., Gao, Y., He, S., 2018. Atlantic multidecadal oscillation modulates the impacts of Arctic Sea ice decline. Geophys. Res. Lett. 45, 2497–2506. https://doi.org/10.1002/2017GL076210.

Loikith, P.C., Detzer, J., Mechoso, C.R., Lee, H., Barkhordarian, A., 2017. The influence of recurrent modes of climate variability on the occurrence of monthly temperature extremes over South America. J. Geophys. Res. 122, 297–311. http://dx.doi.org/10.1002/2017JD027561.

Lovino, M.A., 2015. Environmental Impact of Climate Variability and Extreme Events in the Province of Santa Fe (Argentina), Within the Climate Change Context. Universidad Nacional del Litoral, Argentina (PhD thesis, 238 pp). http://bibliotecavirtual.unl.edu.ar:8080/tesis/handle/11185/707.

Lovino, M.A., García, N., Baethgen, W., 2014. Spatiotemporal analysis of extreme precipitation events in the northeast region of Argentina (NEA). J. Hydrol. 2, 140–158. http://dx.doi.org/10.1016/j.ejrh.2014.09.001.

Lovino, M.A., Müller, O.V., Müller, G.V., Sgroi, L.C., Baethgen, W.E., 2018. Interannual-to-multidecadal hydroclimate variability and its sectoral impacts in northeastern Argentina. Hydrol. Earth Syst. Sci. 22, 3155–3174. http://dx.doi.org/10.5194/hess-22-3155-2018).

Magrin, G.O., Travasso, M.I., Rodriguez, G.R., Solman, S., Nuñez, M., 2009. Climate change and wheat production in Argentina. Int. J. Glob. Warming 1 (1/2/3), 214–226. http://dx.doi.org/10.1504/IJGW.2009.027090.

Magrin, G.O., Travasso, M.I., Mehzer, R., 2012. Impacts of Climate Variability and Extremes on Crop Production in Argentina. Planet Under Pressure 2012, INTA, Argentina Available at: http://elsevier.conference-services.net/programme.asp?conferenceID=2808&action=prog_categories, Accessed date: 18 April 2017.

Magrin, G.O., Marengo, J.A., Boulanger, J.-P., Buckeridge, M.S., Castellanos, E., Poveda, G., Scarano, F.R., Vicuña, S., 2014. Central and South America. In: Barros, V.R., Field, C.B., Dokken, D.J., Mastrandrea, M.D., Mach, K.J., Bilir, T.E., Chatterjee, M., Ebi, K.L., Estrada, Y.O., Genova, R.C., Girma, B., Kissel, E.S., Levy, A.N., MacCracken, S., Mastrandrea, P.R., White, L.L. (Eds.), Climate Change 2014: Impacts, Adaptation, and Vulnerability. Part B: Regional Aspects. Contribution of Working Group II to the Fifth Assessment Report of the Intergovernmental Panel on Climate Change. Cambridge University Press, Cambridge, United Kingdom and New York, NY, USA, pp. 1499–1566.

Marengo, J.A., 2004. Interdecadal variability and trends of rainfall across the Amazon basin. Theor. Appl. Climatol. 78, 79–96. http://dx.doi.org/10.1007/s00704-004-0045-8.

Marengo, J.A., Liebmann, B., Grimm, A.M., Misra, V., Silva Dias, P.L., Cavalcanti, I.F.A., Carvalho, L.M.V., Berbery, E.H., Ambrizzi, T., Vera, C.S., Saulo, A.C., Nogues-Paegle, J., Zipser, E., Seth, A., Alves, L.M., 2012. Recent developments on the south American monsoon system. Int. J. Climatol. 32, 1–21. http://dx.doi.org/10.1002/joc.2254.

Mayer, L.I., Rattalino Edreira, J.I., Navarrete Sánchez, R.A., Maddonni, G.A., Otegui, M.E., 2012. Effect of high temperatures on maize productivity (in Spanish). In: XX Congreso Aapresid "20 veces sí", . http://www.string-agro.com/aapresid/archivo/2012/ponencias/C20_010.pdf, Accessed date: April 2017.

Mo, K.C., Berbery, E.H., 2011. Drought and persistent wet spells over South America based on observations and the U.S. CLIVAR drought experiments. J. Clim. 24, 1801–1820. http://dx.doi.org/10.1175/2010JCLI3874.1.

Moron, V., Vautard, R., Ghil, M., 1998. Trends, interdecadal and interannual oscillations in global sea-surface temperatures. Clim. Dyn. 14, 545–569. http://dx.doi.org/10.1007/s003820050241.

Müller, G., Nuñez, M., Seluchi, M., 2000. Relationship between ENSO cycles and frost events within the pampa Húmeda region. Int. J. Climatol. 20, 1619–1637. http://dx.doi.org/10.1002/1097-0088(20001115)20:13<1619::AID-JOC552>3.0.CO;2-F.

Müller, G.V., Compagnucci, R., Nuñez, M., Salles, A., 2003. Surface circulation associated with frosts in the wet pampas. Int. J. Climatol. 23 (8), 943–961. http://dx.doi.org/10.1002/joc.907.

Müller, O.V., Berbery, E.H., Alcaraz-Segura, D., Ek, M.B., 2014. Regional model simulations of the 2008 drought in southern South America using a consistent set of land surface properties. J. Clim. 27, 6754–6778. http://dx.doi.org/10.1175/JCLI-D-13-00463.1.

National Geographic Institute (NGI), 2015. Geographical Atlas of the Argentine Republic (in Spanish). Distal Editorial, Buenos Aires, Argentina (330 pp. ISBN 9789874571908).

Nogués-Paegle, J., Mechoso, C., Fu, R., Berbery, E.H., Winston, C., Chen, T.-C., Cook, K., Diaz, A., Enfield, D., Ferreira, R., Grimm, A., Kousky, V., Liebmann, B., Marengo, J., Mo, K., Neelin, L., Paegle, J., Robertson, A., Seth, A., Vera, C., Zhou, J., 2002. Progress in Pan American CLIVAR research: understanding the south American monsoon. Meteor-Forschung 27, 3–32.

Okabe, A., Boots, B., Sugihara, K., 2000. Spatial Tessellations Concepts and Applications of Voronoi Diagrams, 2nd ed. John Wiley, New York, United States.

Rasmussen, K.L., Chaplin, M.M., Zuluaga, M.D., Houze, R.A., 2016. Contribution of extreme convective storms to rainfall in South America. J. Hydrometeorol. 17, 353–367. http://dx.doi.org/10.1175/JHM-D-15-0067.1.

Rondanini, D., Mantese, A., Savín, R., Hall, A.J., 2006. Responses of sunflower yield and grain quality to alternating day/night high temperature regimes during grain filling: effects of timing, duration and intensity of exposure to stress. Field Crop Res. 96, 48–62. http://dx.doi.org/10.1016/j.fcr.2005.05.006.

Rusticucci, M., 2012. Observed and simulated variability of extreme temperature events over South America. Atmos. Res. 106, 1–17. http://dx.doi.org/10.1016/j.atmosres.2011.11.001.

Rusticucci, M.M., Kousky, V.E., 2002. A comparative study of maximum and minimum temperatures over Argentina: NCEP-NCAR reanalysis versus station data. J. Clim. 15, 2089–2101. http://dx.doi.org/10.1175/1520-0442(2002)015<2089:ACSOMA>2.0.CO;2.

Rusticucci, M., Kyselý, J., Almeira, G., Lhotka, O., 2015. Long-term variability of heat waves in Argentina and recurrence probability of the severe 2008 heat wave in Buenos Aires. Theor. Appl. Climatol. http://dx.doi.org/10.1007/s00704-015-1445-7.

Rusticucci, M., Barrucand, M., Collazo, S., 2016. Temperature extremes in the Argentina central region and their monthly relationship with the mean circulation and ENSO phases. Int. J. Climatol. http://dx.doi.org/10.1002/joc.4895.

Seager, R., Naik, N., Baethgen, W., Robertson, A., Kushnir, Y., Nakamura, J., Jurburg, S., 2010. Tropical oceanic causes of interannual to multidecadal precipitation variability in Southeast South America over the past century. J. Clim. 23, 5517–5539. http://dx.doi.org/10.1175/2010JCLI3578.1.

Sen, P.K., 1968. Estimates of the regression coefficient based on Kendall's tau. J. Am. Stat. Assoc. 63, 1379–1389.

Seneviratne, S.I., Nicholls, N., Easterling, D., Goodess, C.M., Kanae, S., Kossin, J., Luo, Y., Marengo, J., McInnes, K., Rahimi, M., Reichstein, M., Sorteberg, A., Vera, C., Zhang, X., 2012. Changes in climate extremes and their impacts on the natural physical environment. In: Field, C.B., Barros, V., Stocker, T.F., Qin, D., Dokken, D.J., Ebi, K.L., Mastrandrea, M.D., Mach, K.J., Plattner, G.-K., Allen, S.K., Tignor, M., Midgley, P.M. (Eds.), Managing the Risks of Extreme Events and Disasters to Advance Climate Change Adaptation. A Special Report of Working Groups I and II of the Intergovernmental Panel on Climate Change (IPCC). Cambridge University Press, Cambridge, UK, and New York, NY, USA, pp. 109–230.

Sillmann, J., Kharin, V.V., Zhang, X., Zwiers, F.W., Bronaugh, D., 2013. Climate extremes indices in the CMIP5 multimodel ensemble: part 1. Model evaluation in the present climate. J. Geophys. Res. Atmos. 118, 1716–1733. http://dx.doi.org/10.1002/jgrd.50203.

Silva, V.B., Kousky, V.E., Higgins, R.W., 2011. Daily precipitation statistics for South America: an Intercomparison between NCEP Reanalyses and observations. J. Hydrometeorol. 12, 101–117. http://dx.doi.org/10.1175/2010JHM1303.1.

Skansi, M.M., Brunet, M., Sigró, J., Aguilar, E., Arevalo Groening, J.A., Betancour, O.J., Castellón Geier, Y.R., Correa Amaya, R.L., Jácome, H., Malherios Ramos, A., Oria Rojas, C., Pasten, A., Sallons Mitro, S., Villaroel, C., Martínez, R., Alexander, L.V., Jones, P.D., 2013. Warming and wetting signals emerging from analysis of changes in climate extreme indices over South America. Glob. Planet. Chang. 100, 295–307. http://dx.doi.org/10.1016/j.gloplacha.2012.11.004.

Stocker, T.F., Qin, D., Plattner, G.-K., Alexander, L.V., Allen, S.K., Bindoff, N.L., Bréon, F.-M., Church, J.A., Cubasch, U., Emori, S., Forster, P., Friedlingstein, P., Gillett, N., Gregory, J.M., Hartmann, D.L., Jansen, E., Kirtman, B., Knutti, R., Krishna Kumar, K., Lemke, P., Marotzke, J., Masson-Delmotte, V., Meehl, G.A., Mokhov, I.I., Piao, S., Ramaswamy, V., Randall, D., Rhein, M., Rojas, M., Sabine, C., Shindell, D., Talley, L.D., Vaughan, D.G., Xie, S.-P., 2013. Technical summary. In: Stocker, T.F., Qin, D., Plattner, G.-K., Tignor, M., Allen, S.K., Boschung, J., Nauels, A., Xia, Y., Bex, V., Midgley, P.M. (Eds.), Climate Change 2013: The Physical Science Basis. Contribution of Working Group I to the Fifth Assessment Report of the Intergovernmental Panel on Climate Change. Cambridge University Press, Cambridge, United Kingdom and New York, NY, USA.

Vautard, R., 1995. Patterns in time: SSA and MSSA. In: von Storch, H., Navarra, A. (Eds.), Chapter 14 of Analysis of Climate Variability: Applications of Statistical Techniques. Springer Verlag, Berlin, pp. 327.

Vera, C., Vigliarolo, P.K., Berbery, E.H., 2002. Cold season synoptic scale waves over subtropical South America. Mon. Weather Rev. 130, 684–699. http://dx.doi.org/10.1175/1520-0493(2002)130<0684:CSSSWO>2.0.CO;2.

Verón, S.R., de Abelleyra, D., Lobell, D., 2015. Impacts of precipitation and temperature on crop yields in the pampas. Clim. Chang. 130, 235–245. http://dx.doi.org/10.1007/s10584-015-1350-1.

Virji, H., 1981. A preliminary study of Summer time tropospheric circulation patterns over South America estimated from cloud winds. Mon. Wea. Rev. 109, 599–610. http://dx.doi.org/10.1175/1520-0493(1981)109<0599:APSOST>2.0.CO;2.

Wang, X.L., Swail, V.R., 2001. Changes of extreme wave heights in northern hemisphere oceans and related atmospheric circulation regimes. J. Clim. 14, 2204–2220. http://dx.doi.org/10.1175/1520-0442(2001)014<2204:COEWHI>2.0.CO;2.

Wang, A., Zeng, X., 2012. Evaluation of multireanalysis products with in situ observations over the Tibetan plateau. J. Geophys. Res. 117, D05102. http://dx.doi.org/10.1029/2011JD016553.

Wang, X.L., Chen, H., Wu, Y., Feng, Y., Pu, Q., 2010. New techniques for detection and adjustment of shifts in daily precipitation data series. J. Appl. Meteorol. Climatol. 49 (12), 2416–2436. http://dx.doi.org/10.1175/2010JAMC2376.1.

Wilks, D.S., 2006. Statistical Methods in the Atmospheric Sciences. Elsevier Inc, UK (627 pp).

Winchester, L., Szalachman, R., 2009. The urban poor's vulnerability to the impacts of climate change in latin America and the Caribbean. A policy agenda. In: Presented at the 5th Urban Research Symposium “Cities and Climate Change: Responding to the Urgent Agenda” June 28–30, 2009, Marseille, France. The World Bank, Washington, DC, USA (31 pp). http://siteresources.worldbank.org/INTURBANDEVELOPMENT/Resources/336387-1342044185050/8756911-1342044630817/V2Chap28.pdf.

Wolter, K., Timlin, M.S., 2011. El Niño/southern oscillation behaviour since 1871 as diagnosed in an extended multivariate ENSO index (MEI.ext). Int. J. Climatol. 31, 1074–1087. http://dx.doi.org/10.1002/joc.2336.

Yang, E., Kim, H.M., 2017. Evaluation of a regional reanalysis and ERA-interim over East Asia using in situ observations during 2013–14. J. Appl. Meteorol. Climatol. 56, 2821–2844. http://dx.doi.org/10.1175/JAMC-D-16-0227.1.

Young, K.C., 1992. A three-way model for interpolating monthly precipitation values. Mon. Weather Rev. 120, 2561–2569. http://dx.doi.org/10.1175/1520-0493(1992)120<2561:ATWMFI>2.0.CO;2.

Zaninelli, P., Carril, A.F., Menéndez, C.G., 2015. Exploring maximum and minimum temperatures in different reanalysis. Part 1: means season patterns (in Spanish). Meteor-Forschung 40, 43–58.

Zhang, X., Vincent, L.A., Hogg, W.D., Niitsoo, A., 2000. Temperature and precipitation trends in Canada during the 20th century. Atmosphere-Ocean 38, 395–429. http://dx.doi.org/10.1080/07055900.2000.9649654.

Zhang, X., Hegerl, G., Zwiers, F.W., Kenyon, J., 2005. Avoiding inhomogeneity in percentile-based indices of temperature extremes. J. Clim. 18, 1641–1651. http://dx.doi.org/10.1175/JCLI3366.1.

Zhang, X., Alexander, L.V., Hegerl, G.C., Klein-Tank, A., Peterson, T.C., Trewin, B., Zwiers, F.W., 2011. Indices for monitoring changes in extremes based on daily temperature and precipitation data. Wiley Interdiscip. Rev. Clim. Chang. 2, 851–870. http://dx.doi.org/10.1002/wcc.147.

Zhang, W., Lou, Y., Huang, J., Zheng, F., Cao, Y., Liang, H., Shi, C., Liu, J., 2018. Multiscale variations of precipitable water over china based on 1999–2015 ground-based GPS observations and evaluations of reanalysis products. J. Climate 31, 945–962. http://dx.doi.org/10.1175/JCLI-D-17-0419.1.

Zhou, J., Lau, K., 1998. Does a monsoon climate exist over South America? J. Clim. 11, 1020–1040.

Zipser, E.J., Cecil, D.J., Liu, C., Nesbitt, S.W., Yorty, D.P., 2006. Where are the most intense thunderstorms on earth? Bull. Am. Meteorol. Soc. 87, 1057–1071. http://dx.doi.org/10.1175/BAMS-87-8-1057.